KSHV Episome Tethering Sites on Host Chromosomes: Regulation of Latency-Lytic Switch by the ChAHP complex

Ashish Kumar
UC Davis School of Medicine
Yuanzhi Lyu
UC Davis School of Medicine
Yuichi Yanagihashi
Lifematics
Chanikarn Chantarasrivong
Lifematics
Vladimir Majerciak
National Cancer Institute https://orcid.org/0000-0003-2907-4583
Michelle Salemi
University of California, Davis
Kang-Hsin Wang
UC Davis
Frank Chuang
UC Davis
Ryan Davis
UC Davis https://orcid.org/0000-0001-7439-6683
Clifford Tepper
UC Davis https://orcid.org/0000-0001-7105-1102
Kazushi Nakano
Lifematics
Chie Izumiya
UC Davis
Michiko Shimoda
UC Davis
Ken-ichi Nakajima
UC Davis
Alexander Merleev
UC Davis
Zhi-Ming Zheng

Tumor Virus RNA Biology Section, HIV Dynamics and Replication Program, Center for Cancer Research, National Cancer Institute, National Institutes of Health, Frederick, MD 21702, USA

Mel Campbell

UC Davis https://orcid.org/0000-0002-8475-6686

Yoshihiro Izumiya (YIZUMIYA@UCDAVIS.EDU)

UC Davis School of Medicine https://orcid.org/0000-0002-9184-2603

Article

Keywords: LANA, ChAHP, KSHV, Episome Tethering Sites

Posted Date: September 22nd, 2021

DOI: https://doi.org/10.21203/rs.3.rs-136834/v2

KSHV Episome Tethering Sites on Host Chromosomes: Regulation of Latency-Lytic Switch by the ChAHP complex

Ashish Kumar[1, #], Yuanzhi Lyu[1, #], Yuichi Yanagihashi[2, #], Chanikarn Chantarasrivong[2], Vladimir Majerciak[3], Michelle Salemi[4], Kang-Hsin Wang[1], Frank Chuang[5], Ryan R. Davis[6], Clifford G. Tepper[5, 7], Kazushi Nakano[2], Chie Izumiya[1], Michiko Shimoda[1, 7], Ken-ichi Nakajima[1], Alexander Merleev[1], Zhi-Ming Zheng[3], Mel Campbell[1,*], & Yoshihiro Izumiya[1,5,7,*]

[1] Department of Dermatology School of Medicine, University of California Davis (UC Davis), Sacramento, California USA

[2] Lifescience Division, Lifematics, Osaka, 541-0046 Japan

[3] HIV Dynamic and Replication Program, National Cancer Institute, NIH, Frederick, Maryland, USA

[4] Genome Center, Proteomics Core, Genome and Biomedical Sciences Facility, UC Davis, Davis, California, USA

[5] Department of Biochemistry and Molecular Medicine, School of Medicine, UC Davis, Sacramento, California USA

[6] Department of Pathology and Laboratory Medicine, School of Medicine, UC Davis, Sacramento, California USA

[7] Viral Oncology and Pathogen-Associated Malignancies Initiative, UC Davis Comprehensive Cancer Center, Sacramento, California USA

[#] These authors contributed equally.

* Correspondence: Mel Campbell, PhD
Address: UCDMC Research III, Room 3300D, 4645 2nd Avenue, Sacramento CA 95817
E. mail: mcampbell@ucdavis.edu
Phone: 916-734-7811

*Correspondence: Yoshihiro Izumiya DVM, PhD
Address: UCDMC Research III, Room 2200B, 4645 2nd Avenue, Sacramento CA 95817
E. mail: yizumiya@ucdavis.edu
Phone: 916-734-7253

Word counts:

Abstract: 150

Abstract

Kaposi's sarcoma-associated herpesvirus (KSHV) establishes a latent infection in the cell nucleus, but where KSHV episomal genomes are tethered and the mechanisms underlying KSHV lytic reactivation are unclear. Here, we study the nuclear microenvironment of KSHV episomes and show that the KSHV latency-lytic replication switch is regulated via viral long non-coding (lnc)RNA-CHD4 (chromodomain helicase DNA binding protein 4) interaction. KSHV episomes localize with a CHD4 complex, ChAHP, at epigenetically active genomic regions and tethers frequently near centromeric regions of host chromosomes. The ChAHP complex also occupies the 5'-region of a highly-inducible lncRNAs and terminal repeats of KSHV genome with latency-associated nuclear antigen (LANA). Viral lncRNA binding competes with CHD4 DNA binding, and KSHV reactivation is accompanied by the detachment of KSHV episomes from host chromosome docking sites We propose a model in which elevated lncRNA expression determines the KSHV latency-lytic decision by regulating LANA/ChAHP DNA binding at inducible viral enhancers.

Introduction

Kaposi's sarcoma-associated herpesvirus (KSHV), discovered in 1994, is one of eight human herpesviruses (1). Since then, KSHV has been identified as the causative agent of Kaposi's sarcoma (1-3) and two human lymphoproliferative diseases, primary effusion lymphoma (PEL) and AIDS-related multicentric Castleman's disease (4-7). Although HAART (highly active antiretroviral therapy) of HIV-patients dramatically reduced KS incidence in Western countries, KSHV associated-malignancies are still a leading cause of cancer deaths in AIDS patients in Sub-Saharan Africa. Additional therapeutic measures are urgently needed. In cancer cells, KSHV establishes a latent infection in which most viral genes are silenced with the exception of few latent proteins, such as latency associated nuclear antigen (LANA) (8). External stimuli trigger KSHV reactivation in latently infected cells through activation of highly potent viral transactivator, K-Rta, which then activates early gene expression including three viral long non-coding RNAs (9-11).

KSHV LANA is a 130 kDa multifunctional protein, which plays a major role in both DNA replication and episome maintenance during latency. LANA binds DNA sequences within the 801 base pair terminal repeats (TRs) of the KSHV genome, which serve as both an origin of DNA replication and a site for tethering episomes to the host cell chromosomes (12-15). There are two distinct mechanisms through which LANA tethers episomes to host cell chromosomes. First, the N-terminus of LANA, which is predicted to be highly-unstructured, can interact with host chromosomes through direct binding with histone H2A and H2B (16, 17). A second mechanism involves the interaction of the LANA DNA binding domain (DBD) with host chromatin-associated proteins (18-20). The chromatin-associated proteins include BRD2 and BRD4, which contain two bromodomains that recognize the acetylated H3 and H4 histones, and

77 a conserved C-terminal extraterminal domain (21, 22). The BRD extraterminal domain interacts
78 directly with the LANA DBD, providing a putative mechanism for episome docking sites selection
79 at epigenetically active host chromosomes (18, 23). In both mechanisms, tethering requires a
80 sequence-specific interaction between the LANA DBD and the viral episome at LANA binding
81 sites 1 and 2 (LBS 1/2) (15). Episome maintenance requires at least two copies of LBS1/2 and
82 the KSHV genome encodes 30 to 40 terminal repeats, taking up to approximately one fifth of
83 KSHV genome (24-32 kbp DNA fragment) (24). The crystal structures of the LANA DBD further
84 revealed that LANA can form a higher-order decameric ring structure, and a hydrophobic
85 interface between LANA dimers to form the decameric ring is important for cooperative LBS1/2
86 binding, DNA replication, and thereof episome maintenance (25). The crystal structure of LANA
87 DBD also reveals distinct binding interfaces among BRD2/4 binding site, DNA binding, and
88 decameric interfaces (25, 26).

89 Spatial and temporal organization of the genome plays a critical role in gene expression
90 in many organisms including large DNA viruses (27, 28). Similar to cellular genes, the KSHV
91 episome changes its genomic structure with increasing genomic looping at KSHV Replication
92 and Transactivation (K-Rta) binding sites during KSHV reactivation (28). Imaging studies
93 suggested that DNA/RNA/protein aggregates are formed at actively transcribed sites, in which
94 a significant fraction of RNA Polymerase II (RNAPII) is recruited to the KSHV genomes and used
95 to transcribe viral genomes during KSHV reactivation (29). Such transcription factory formation
96 is known to bring gene promoters and enhancers together (27). It is clear that dynamic regulation
97 of genome architecture plays a critical role in gene transcription, hence outcomes of KSHV
98 latency-lytic replication decisions. However, the mechanisms that control KSHV episome
99 architecture remains elusive.

Chromatin remodeling enzymes have been of wide interest in the regulation of KSHV latency-lytic switch. The enzymes include polycomb repressor complex 1 and 2, nucleosome remodeling and deacetylase (NuRD), lysine demethylases (KDM2B, 3A, and 4A), histone lysine acetylase and methylases (20, 30-35). Recent studies highlight that chromatin remodeling enzymes also participate in regulation of genome architecture. In murine embryonic stem cells, the Iswi family remodeler Snf2h promotes CTCF binding to the genome and regulates formation of contact domains (36, 37). In addition to Snf2h, CHD4 (chromo domain helicase DNA binding protein 4) has recently been shown to occupy and restrict enhancer accessibility as well as cohesin occupancy at CHD4 binding sites (38). Genetic disruption of CHD4 therefore causes spontaneous differentiation concomitant with premature activation of lineage-specific genes (39-41). CHD4 has been identified in two distinct cellular protein complexes, the NuRD and ChAHP complexes (42). The ChAHP complex consists of CHD4, ADNP (activity-dependent neuroprotective protein), and HP1γ (heterochromatin protein 1) (39). ANDP binds DNA sequence motifs such as *GCCCTCTTCTGG* and anchors the ChAHP complex to euchromatin (43). ChAHP complex was shown to modulate spatial chromatin loop organization locally, and counteract chromatin looping at CTCF sites (43). Accordingly, ChAHP plays essential roles in maintaining distinct cellular states and ensure accurate cell fate decisions in response to external signals during development that are likely to associate with its function in regulation of enhancer accessibility (39, 41, 44). Because of CHD4's roles in enhancer regulation, it is not surprising that mutation or overexpression of CHD4 has been linked to multiple developmental disorders and malignancies in humans (45-48).

The long non-coding (lnc)RNAs that are transcribed from active enhancers in a cell- or tissue- specific manner are called enhancer RNAs (eRNAs) (49). The functions of eRNAs are

largely mediated through interactions with eRNA binding partners (50-52); however, studies also indicated that RNA sequence is not contributing to the specificity of eRNA-protein interactions. Instead, specificity of the function is suggested to be achieved through gene/RNA positioning and spatial proximity to regulated genomic regions (53). Similarly, the KSHV genome encodes at least three highly inducible lncRNAs (Ori-RNA [also called T1.5], Poly Adenylated Nuclear RNA [PAN RNA], and T0.7) that are transcribed from epigenetically active regions, and are direct targets of K-Rta (11). The PAN RNA genomic locus actively recruits cellular RNAPII during KSHV reactivation, leading to significantly higher copy number of PAN RNA molecules (up to 10^5 copies) in a reactivating cell (54). The high copy number of PAN RNA has also been explained by its higher RNA stability (55). Three sequence elements, ENE (expression and nuclear retention element) at the 3' region, MRE (Mta responsive element) at the 5' region of PAN RNA, and the structure of the poly (A) tail, are critical for PAN RNA stability (56-58). PAN RNA interacts with multiple cellular and viral proteins (57, 59), and functions as a transactivator by sequestering repressors and/or recruiting histone modifying enzymes (32, 60, 61). A recent report shows that PAN RNA could be replaced by other viral lncRNA sequences without a significant loss of KSHV replication, suggesting that there is a sequence-independent function similar to that of eRNAs (62).

In this study, we provide evidence that the KSHV latent-lytic switch is regulated by the ChAHP complex. We mapped KSHV episome tethering sites on host chromosomes with Capture Hi-C and studied the surrounding nuclear microenvironment of KSHV episomes using proximity biotin labeling. We show that KSHV episomes co-localize with the ChAHP complex at epigenetically active host chromosomes, and CHD4 interaction with viral lncRNAs regulates binding of CHD4 on KSHV chromosomes, which de-represses viral lncRNAs from ChAHP-

mediated repression. We propose that the inducible enhancer activity is regulated by a balance between local eRNA transcription activity and ChAHP complex tethering, and the mechanism regulates KSHV reactivation.

Results

Identification of KSHV episome tethering site on host chromosomes.

KSHV episomes tether to the host cell chromosomes via LANA, however the mechanism of selection of docking sites is not very well characterized. To understand how and where KSHV episomes tether to host chromosomes, we applied Capture Hi-C (CHi-C) method to identify episome docking sites in three KSHV naturally-infected PEL cell lines, BC-1, BC-3 and BCBL-1. The schematic diagram for the CHi-C procedure is presented in **Fig. 1a**. In order to obtain high resolution, the Hi-C sequencing library was further enriched by using biotinylated tiling-oligo probes that specifically hybridized to KSHV DNA sequences (**Fig. 1a**). Using this method, we examined the position of host genomic regions that exhibited higher frequencies of normalized chimeric ligation reads with KSHV DNA fragments. We identified selectively enriched chimeric ligation reads throughout the host chromosomes (**Fig. 1b**). The mapped reads on 23 individual chromosomes for BC-1, BC-3 and BCBL-1 are presented separately in **Supplementary Fig. 1a-c**. Each dot represents the number of normalized contact heterotypic sequence reads between host and KSHV sequences. The CHi-C normalized chimeric read counts on chromosome 1 for three naturally infected PEL cells are shown in **Fig. 1c**. The results indicated that there are a higher number of chimeric read counts near centromeric regions in all three cell lines (**Fig. 1c**). To study the frequencies of chimeric read counts that are located near the centromere region,

we performed a mathematic characterization, in which we extracted the chimeric read counts that derived from regions spanning a distance corresponding to 1% of the size of each chromosome at either 5' or 3' centromere chromosome regions (marked green and blue). Counts per 100 kbp were calculated separately for each chromosome and compared to the average number across the individual chromosome. The results showed that higher chimeric read counts were seen (15 out of 23 chromosomes in BCBL-1) either 5' or 3' regions of centromere, and in some instances (e.g., chromosome 8, 19, X), we observed enrichment in both 5' and 3' positions (**Fig. 1d**). To further confirm the CHi-C findings, we performed DNA-FISH with centromere-specific PNA (peptide nucleic acid) probes in combination with LANA immunostaining. These results further showed that a large fraction of LANA dots was colocalized with centromeres (**Fig. 1e, Supplementary Fig. 2**). The results are consistent with a previous report, which demonstrated that LANA colocalized with centromeric protein F (CENPF) and kinetochore protein, Bub1, and observed at centromere regions during metaphase (63). To determine whether KSHV docking sites are random, we next examined the similarity of KSHV episome tethering sites among the three cell lines using a Jaccard Index. We calculated the similarity of tethering sites based on the positions of chimeric sequence reads. The index identified 97.86% (BC-1 vs BC-3), 81.99% (BC-1 vs BCBL-1) and 82.36% (BC-3 vs BCBL-1) similarity (**Fig. 1f**). The results demonstrated that a majority of KSHV episomes tethers the similar host genomic regions in three naturally infected PEL cell lines, suggesting that there is a preferential nuclear microenvironment that can attract/maintain KSHV latent episomes during cell divisions.

Identification of proteins in close proximity to KSHV latency associated nuclear antigen (LANA).

Next, we examined the nuclear protein microenvironment of KSHV episome-tethering sites in infected cells. We hypothesized that, by examining cellular proteins neighboring to LANA in infected cells, we should be able to identify the repertoire of proteins important for tethering and selection of KSHV episome-docking sites. To identify proteins in close proximity to LANA, we used a miniTurboID based method. The miniTurboID is a biotin ligase, which covalently attaches biotin to lysine residues in neighboring proteins (<10 nm) in less than 10 minutes with no significant cell toxicity (64, 65). A recombinant KSHV BAC16 with LANA N-terminal tagged with miniTurboID (referred to as KSHV LANA-mTID) was prepared; the procedure for the preparation of KSHV LANA-mTID is presented in **Supplementary Fig. 3**. We transfected the *i*SLK cells with the recombinant KSHV LANA-mTID and stably selected with hygromycin (1 mg/ml). The KSHV LANA-mTID virus was then recovered by inducing reactivation with doxycycline (1 μg/ml) and sodium butyrate (3 mM) for 5 days. *i*SLK cell line was infected with recombinant KSHV LANA-mTID virus and selected with hygromycin (1 mg/ml) to generate stable *i*SLK-LANA mTID cells (**Fig. 2a**). The *i*SLK-LANA mTID cells were incubated with D-biotin for 60 minutes in culture media and biological triplicated samples were prepared (**Fig. 2b)**. This strategy led us to identify 76 host proteins ($P<0.05$) that were physically neighboring KSHV LANA within 10 nm radial distance during the period of D-biotin incubation (64). The 76-host proteins include nuclear mitotic apparatus protein (NuMA), bromodomain-containing protein 4 (BRD4), and lysine-specific demethylase 3A and 3B (KDM3A and 3B) that have been previously shown to physically interact with LANA (20, 66-68) (**Fig. 2c, Supplementary Table 1**). In addition to those previously identified cellular proteins, the study also precipitated components of the ChAHP complex (39), which is composed of chromodomain helicase DNA-binding protein 4 (CHD4), Activity-dependent neuroprotector homeobox protein (ADNP) and HP-1γ with high confidence (**Fig. 2c**).

214 Although we could not identify HP-1γ with our statistical criterion in proteomics study, HP-1γ
215 protein was previously shown to interact with KSHV LANA (69). The LANA interaction with CHD4
216 and ADNP was further validated with *in vitro* pull-down assays, and the results showed that
217 LANA could interact with CHD4 and ADNP in the absence of other viral proteins (**Fig. 2d**).
218 Further, recombinant GST-tagged LANA deletion proteins (**Supplementary Fig. 4**) were used
219 to map the interaction domain with CHD4 and found that the amino acid (aa) residues 870-1070,
220 near the LANA DNA-binding domain, were responsible for interaction with CHD4 (**Fig. 2e**).
221 Immunofluorescence assays with mono-specific antibodies further confirmed that LANA and
222 CHD4 were colocalized in naturally infected BCBL-1 cells (**Fig. 2f**). Taken together, these results
223 suggest that LANA is able to associate with the ChAHP complex in latently infected cells.

224

225 **Association of KSHV episome-tethering sites with ChAHP complex binding.**

226 The protein interaction and colocalization between CHD4 and LANA "dots" in the nucleus led us
227 to further investigate the localization of CHD4, ADNP and LANA on both host and KSHV
228 chromosomes. To identify the chromatin occupancy site(s) for ChAHP complex and LANA, we
229 employed Cleavage Under Targets and Release Using Nuclease (CUT&RUN) (70). The LANA,
230 CHD4, and ADNP CUT&RUN peaks clearly overlapped at multiple sites of cell host
231 chromosomes with active histone marks (H3K27Ac), which include previously described IRF4
232 super enhancer region (71, 72) (**Fig. 3a**). NGS plots between LANA CUT&RUN summit peaks,
233 and CHD4 or ADNP further confirmed co-occupancies of LANA and the ChAHP complex on the
234 host chromosomes (**Fig. 3b**). Because LANA and ChAHP complex interact with each other, we
235 hypothesized that LANA-ChAHP complex could be important for tethering KSHV episomes to
236 host chromosomes. To test this, we generated NGS plots between LANA, CHD4 and ADNP

CUT&RUN summit peaks, and distribution of CHi-C chimeric reads. We observed that KSHV episome tethering sites were indeed primarily localized near the LANA, CHD4 and ADNP binding sites, whereas it was not observed for H3K4me1 (**Fig. 3c**) or H3K27me3 (**data not shown**). To further calculate degree of interaction mathematically, we measured the relative CHi-C chimeric reads per million and examined association with relative distance with CHD4 binding site. Accumulation index calculated from NGS plot suggested that more than 50% of CHi-C reads are closely located at CHD4 binding site within the genomic regions (**Fig. 3d**). Altogether, these results suggest that KSHV episome tethers to host chromosome at the ChAHP binding sites.

KSHV LANA colocalization with ChAHP complex on KSHV genome.

We next examined ChAHP binding sites on the KSHV episome. Consistent with studies with cellular chromosomes, CHD4 and ADNP occupy genomic loci with active histone marks, which includes KSHV long non-coding RNAs (PAN RNA, T0.7, and T1.5 [Ori-RNA]) promoter regions (**Fig. 4a**). The results also showed colocalization among LANA, CHD4, and ADNP with the active histone mark, H3K27Ac, along the KSHV genome, and exceptionally strong peaks were seen at terminal repeat regions (read counts are depicted in Fig. 4a), where multiple copies of LANA bind (73). The strong peaks at TR regions are likely due to a combination of tighter binding of the complex and the presence of multiple copies of the same sequences. The strong signals at TR regions are unlikely due to mapping problems, because H3K27me3 showed a lower number of sequence reads compared with sequence reads in the unique region. The three viral lncRNAs, especially PAN RNA, are known to be expressed at significantly higher transcript copy numbers than the open reading frames during lytic replication (54, 74), and CHD4, ADNP, and LANA were clearly localized at the 5' regions of these lncRNA promoter regions (**Fig. 4a**). Next, the effects

of KSHV reactivation on CHD4 occupancies were examined by CUT&RUN with qPCR. The results suggested that CHD4 occupancies on the KSHV genome were reduced during KSHV reactivation **(Fig. 4b).** We further studied effects of KSHV reactivation on the KSHV episome tethering with the ChAHP complex on host cell chromosomes. For this, TREx-BCBL-1 cells were reactivated for twenty-four hours and CHi-C samples were prepared. We measured the relative chimeric DNA sequence frequencies of KSHV with host chromosomes before and after KSHV reactivation. The relative amount of chimeric sequence reads at one of the KSHV episome tethering sites were visualized with Juicebox. By subtracting the number of relative sequence reads in latent samples from those in reactivated samples, we also visualized changes by induction of active viral transcription. The results showed that KSHV chimeric sequence reads were reduced, suggesting that KSHV reactivation induced detachment of the KSHV episome from host chromosomes, and a similar detachment was also seen in other putative episome-tethering sites **(Fig. 4c).** The results suggest that robust viral lncRNAs at the ChAHP binding site may play a role in detachment of ChAHP/LANA complex from chromosomes.

Identification of PAN RNA binding proteins with proximity biotin ligation.

Previous studies including ours suggested that PAN RNA transcription *in cis* plays an essential role in initiation of KSHV lytic replication. Inhibition of PAN RNA transcription by either deletion of the PAN RNA sequence or mutation at K-Rta responsive elements in the PAN RNA promoter significantly impaired KSHV reactivation and replication (28, 60). In addition, CHD4 is known to bind cellular enhancers to regulate enhancer-promoter interactions, and enhancers often transcribed enhancer RNAs (lncRNAs) (75). To examine PAN RNA-mediated transcription regulation, we again applied the proximity labeling technique to profile PAN RNA neighboring

proteins during KSHV reactivation. This time, the mTID cassette was first inserted as an N-terminal fusion of ORF57, a PAN RNA binding protein, and then the fusion protein was expressed from the endogenous promoter during KSHV reactivation **(Fig. 5a)**. Taking advantage of a previous detailed mapping study, which identified ORF57 binding sites on PAN RNA, termed MRE (Mta Responsive Element) (57), we utilized a PAN MRE mutant virus having a 9-nucleotide mutation in the MRE element **(Fig. 5a)**. KSHV genome-wide qRT-PCR array analysis confirmed previous studies that the PAN RNA MRE mutation impaired viral gene expression, with stronger effects being seen in late gene cluster regions **(Supplementary Fig. 5a right panel)**. We also confirmed that protein biotinylation happened only in the presence of both ORF57 protein (reactivated sample) and biotin **(Fig. 5b)**. By comparing the enrichment profiling between the PAN RNA MRE mutant and PAN RNA Wt, we isolated cellular proteins that are in proximity to ORF57 protein via PAN RNA binding. Proximity biotin labeling identified a total of 129 and 307 proteins from mTID-57 PAN Wt *i*SLK cells and mTID-57 PAN-MRE *i*SLK cells, respectively ($p<0.05$) **(Supplementary Table 2)**. Among the interacting proteins, 74 proteins were common between the PAN MRE Wt and PAN MRE mutant, while 55 proteins were found only in the presence of the wild type PAN RNA sequence **(Fig. 5c, d)**. Deletion of MRE seemed to unleash ORF57 protein and allow ORF57 to interact more freely with other RNA binding proteins (**Fig. 5c**). Importantly, this proteomics approach identified CHD4 as a putative PAN RNA binding protein ($p<0.005$)**.** Next, we performed the siRNA screening of 129 (55 + 74) PAN RNA binding proteins with KSHV reactivation indicator cell line, *i*SLK.219. The knockdown screening identified 4 strong repressors namely IK, CHD4, PABPC3 and RPL18A with fold change (RFP/GFP) > 3 among the 129 proteins, and CHD4 was found be the strongest among them (RFP/GFP > 7-fold) (**Fig. 5e**). Gene Ontology (GO) analysis of 129 PAN RNA-mediated ORF57-interacting

proteins suggested that ORF57 is indeed primarily involved in RNA processing **(Supplementary Fig. 5b)**.

A viral lncRNA inhibits CHD4 dsDNA binding.

PAN RNA MRE-dependent enrichment by ORF57-mediated biotinylation suggested that CHD4 is an RNA-binding protein, and that PAN RNA brings the CHD4 and ORF57 proteins into proximity by serving as a scaffold for the biotinylation (model shown in **Fig. 5a**). In order to examine the interaction of CHD4 with PAN RNA, we prepared purified RNAs (PAN RNA, MRE mutant, PAN RNA deletion mutants and luciferase RNA) and proteins (CHD4, NF-κB and Luciferase) **(Fig. 5f)** and performed *in vitro* interaction assays (**depicted in Fig. 5g**). The results showed that CHD4 was indeed precipitated with PAN RNA; however, MRE mutant, PAN RNA deletion mutants, as well as irrelevant luciferase RNA also interacted with CHD4 protein, suggesting that CHD4 RNA binding is unlikely sequence specific under our binding conditions **(Fig. 5h)**. However, the same RNA binding conditions with full length PAN RNA did not precipitate a DNA binding protein, NF-κB (p65) or Luciferase protein, suggesting that CHD4 does possess RNA-binding capacity **(Fig. 5i)**. Because a previous study showed that Drosophila melanogaster CHD4 homolog is capable of binding DNA and human CHD4 ATPase activity is stimulated in the presence of naked DNA (76), we tested if purified CHD4 protein is able to bind to double stranded (ds)DNA fragment encoding the PAN RNA sequence. Biotinylated primer was used to amplify DNA fragment from the PAN RNA gene and used for biotin-pull down analyses. The results showed that CHD4 was able to bind dsDNA directly **(Fig. 5j)**. Importantly, increasing amounts of PAN RNA (ssRNA) antagonized CHD4 dsDNA binding, which was completely blocked in presence of non-biotinylated PAN RNA at 1:10 (dsDNA/RNA) molecular

ratio **(Fig. 5j)**. The results suggested that locally transcribing long non-coding RNAs (which would reach up to $3x10^5$ copies/cell for PAN RNA (54)) may remove CHD4 locally from the KSHV genome, as seen by reduced CHD4 on KSHV genome **(Fig. 4b)** and detachment of KSHV episomes from host chromosomes during reactivation **(Fig. 4c)**. These results suggest that amount of long non-coding RNAs expression near the CHD4 binding sites may play a role in both lytic gene induction and episome tethering.

CHD4 is important for latency maintenance and establishment.

The studies above suggest that LANA interacts with the ChAHP complex on both cellular and viral chromosomes, and that the ChAHP complex may restrict KSHV enhancer activity and hence KSHV lytic reactivation. Accordingly, we next examined the significance of CHD4 in the KSHV transcription program. CHD4 expression in *i*SLK.219 cell was knocked down with shRNA and the degree of KSHV reactivation was examined after triggering K-Rta expression with doxycycline. The results showed that knock-down of CHD4 enhanced KSHV replication more than 8-fold over K-Rta induction alone. Conversely, functional re-introduction of CHD4 by over expression of mouse *Chd4* cDNA (i.e., in order to escape from the shRNA, which targets human CHD4) counteracted effects of CHD4 knock-down (**Fig. 6a**). Notably, over expression of mouse Chd4 almost completely abolished K-Rta mediated KSHV reactivation (**Fig. 6a, second bar**), and inhibited the aggregation of RNAPII on the KSHV genome, which was measured by immunostaining with overexpressed CHD4 and RNAPII (**Fig. 6b**). Strong silencing effects were CHD4's ATPase-activity dependent, because mutations in the helicase domain, using the same mutation found in patients with CHD4-associated syndrome (42, 77), was found to increase RNAPII aggregation and KSHV transcription **(Fig. 6b, c)**. In addition to the knock-down or over

expression studies, we also performed single cell transcriptomic studies with reactivated *i*SLK.219 cells. The results clearly indicated that the presence of higher levels of CHD4 had clear inhibitory effects for the triggering and/or prolonging lytic viral gene transcription burst **(Fig. 6d)**. Further, KSHV transcripts were extracted and sorted based on sequence counts and examined for correlation with cellular gene expression at the single cell level **(Supplementary Fig. 6a, b).** The results again showed a negative correlation between CHD4 expression and the amount of KSHV transcripts in the cell **(Fig. 6e),** while a similar negative correlation was not observed for GAPDH or similarly expressing HDAC2, a component of NuRD complex (**Supplementary Fig. 6c**).

Finally, the significance of CHD4 in the establishment of latency was also examined. To do this, we first knocked-down CHD4 in 293T cells and infected the cells with purified KSHV r.219 virus to monitor viral gene silencing. CHD4 knock-down was confirmed at the protein and RNA levels **(Fig. 6f, g)**. The results showed that KSHV gene expression continued to increase during a 3-day period in two independent CHD4 KD cells, while KSHV gene expression did not increased significantly in shScramble cells at day 3 (**Fig. 6h**). Further, KSHV lytic replication was also monitored with RFP signals within the cell population, and results showed that the number of RFP positive cells within the dish were higher in CHD4 knock-down 293T cells compared to negative control knock-down (siC) cells at 96 hours post infection **(Fig. 6i, Supplementary Fig. 7)**. Altogether, these results suggest that CHD4 functions to silence KSHV lytic genes at an early stage of KSHV *de novo* infection and facilitate the entry and maintenance of latency, perhaps by suppressing robust viral lncRNA expression for the viral enhancer activity.

Discussion

Recent exciting studies suggest that an RNA-binding domain in transcription factor CTCF is essential for the formation of subsets of genome architecture (78, 79). The presence of distinct classes of RNA-binding protein (RBP)-dependent genomic loop formation suggests the partition of nascent RNAs and other RBP partners in chromatin-looping regulation at transcriptionally active genomic loci. It is also known that eRNAs and RNA-binding proteins participate in transcriptional factories (75, 80, 81). We show here that overexpression of CHD4 prevents RNAPII aggregate formation and inhibits KSHV reactivation **(Fig. 6a,b)**. Regulation of the KSHV latency-lytic switch by CHD4 chromatin binding and inhibition of CHD4 DNA binding via inducible transcription in cis may necessitate for KSHV to evolutionally maintain the viral nuclear lncRNAs, which are often expressed at levels 1,000x greater than the majority of KSHV protein-coding RNAs during reactivation (54). Evolution of this RNA as a nuclear and non-coding species may also avoid competition for protein translation and RNA export machineries, while functioning to trigger robust enhancer activity for KSHV genome. Consistent with CHD4 being a strong repressor, loss-of-function mutations induce enhancer activation leakage, which associates with multiple developmental disorders in humans (44, 47, 82-85). We think that such CHD4 functional loss may result in an increased propensity to form active enhancer-promoter interactions and prolong gene transcription similar to our observations in KSHV-infected CHD4-KD 293T cells (**Fig. 6h**). Consistent with CHD4 functions in enhancer access restriction, the ChAHP complex is also known to compete with CTCF binding, and counteract chromatin looping at CTCF binding sites. Therefore, ChAHP maintains evolutionarily conserved spatial chromatin organization by preventing new CTCF binding events that emerged through short Interspersed element expansions (43); this ChAHP biological role suggests that KSHV cleverly find/build a “safe basecamp” with ChAHP to maintain viral episomes structure during evolution.

A study from Dr. Lieberman's group demonstrated that EBV episomes are tethered in the neighborhood of transcriptionally silent neuronal genes (86). Our CHi-C study also found KSHV episomes frequently localize at the junctions between eu- and hetero-chromatin (**Supplementary Fig. 8** - junction of stripes), but more frequently localizes near centromere regions than to other genomic regions. The advantage of tethering at near centromere remains unknown; however, previous studies also showed that LANA dots are localized at centromeres and LANA interact with centromeric protein F and kinetochore protein, Bub1(63); the two proteins may play a role in recruitment of KSHV episomes to the unique genomic regions through interaction with LANA.

The siRNA screening for epigenetic factors, which have a significant impact on KSHV replication has been reported (30). The report showed that CHD4 is indeed a suppressor for KSHV lytic replication. Here, we further showed that KSHV episomes are localized with ChAHP on host chromatin and interact with LANA at the hydrophobic interface of LANA dimers near the LANA DNA binding domain (25, 26). Suppression of KSHV lytic genes by CHD4 in *de novo* infected cells also suggests that there might be active recruitment of the ChAHP complex to the incoming KSHV genomes. However, the mechanism(s) that enable KSHV episomes to select specific ChAHP binding sites on host chromosomes, and whether these CHD4 occupied enhancers are linked to tissue-specific gene expression therefore KSHV tissue tropism have yet to be characterized. At least in the three PEL cell lines examined, one of the common ChAHP-LANA complex-recruitment site is IRF4 super enhancer region, which is highly active in the B-cell lineage (71, 72, 87). It will be important to know if KSHV episome-bound cellular “enhancers” are annexed and subjected to control by KSHV proteins in infected cells.

KSHV has been evolved to maintain a mysterious lncRNA, PAN RNA, which is expressed at a very high copy number in the presence of ORF57 protein (54), and deletion of PAN RNA or ORF57 significantly impairs the entire viral lytic gene expression program (28, 60, 88). How PAN RNA expression activates the expression of distantly localized viral open reading frames is an important question. Because PAN RNAs exceeds 10^5 copies, and CHD4 localizes at PAN RNA transcription initiation sites with LANA (**Fig. 4a**), we expect that the local PAN RNA concentration would easily result in an RNA-DNA ratio in excess of 10:1 in presence of ORF57 (57). Based on frequent genomic looping, non-coding RNA expression, and CHD4 binding (e.g., which frequently targets enhancers), we propose that the lncRNA encoding regions [Ori-RNA (T1.5), PAN RNA, K12 (T0.7)] function as inducible enhancers for expression of the KSHV ORFs, and KSHV reactivation (e.g., promoter activation) hinges on lncRNA-CHD4 interactions for the de-repression. Similar to CHD4, we previously demonstrated that PAN RNA expression also sequesters LANA from unique regions of KSHV genomes (61). Our CUT&RUN studies showed that CHD4 and LANA colocalized on both the KSHV and host genomes (**Fig. 4a**) and they could physically interact with each other (**Fig. 2d-f**); thus, we favor the idea that reactivation is triggered by detachment of LANA/ChAHP complex-loaded TR fragments from the KSHV unique region (ORFs-encoded region as well as host chromosome) by robust expression of lncRNA, whose expression is directly activated by K-Rta and enhanced by ORF57. In this proposed model, transcriptional burst by a strong viral transactivator, results in the local appearance of multiple nascent and stable-RNA copies simultaneously, in turn increasing local nucleic acid density before PAN RNA is diffused into the nuclear neighborhood. Notably, our KSHV 3D genomic structure modeling based on frequencies of CHi-C reads within KSHV sequences suggested that these highly inducible lncRNA encoding regions localize spatially in close proximity to TRs

in 3D (**Model in Fig. 6j**, Campbell et al., in preparation). The results combined with this study suggest that the ChAHP-LANA complex has an architectural role for KSHV latent genomic structure, and the TR region that recruits significant number of copies of both ChAHP and LANA (**Fig. 4a**) is critical for episome structure and therefore suppression of lytic genes epigenetically. Disruption of such a "backbone" by CHD4 KD or by robust expression of PAN RNA which binds CHD4 therefore triggers "leakage" of viral lytic gene expression similarly to premature activation of lineage-specific genes [(39-41) and **Fig. 6g**)]. Structural studies for the ChAHP/LANA protein complex with TR unit and recombinant KSHV with a LANA CHD4 binding mutant would further clarify the significance of the interaction and possibly lead to small molecular drugs to target the interaction.

In summary, we have demonstrated that the ChAHP complex is a key regulator of the KSHV latency-lytic switch. With strong effects of CHD4 on KSHV replication, it will be important to study how ChAHP complexes are regulated in infected cells, and also a relationship with KSHV replication and KSHV-mediated disease progression in individuals who unfortunately possess CHD4 mutations.

Methods

Materials. Dulbecco's Modified Eagle medium (DMEM), RPMI 1640 medium, fetal bovine serum (FBS), phosphate buffered saline (PBS), Trypsin-EDTA solution, 100x Penicillin-streptomycin-L-glutamine solution and Streptavidin-HRP conjugate were purchased from Thermo Fisher Scientific (Waltham, MA USA). Puromycin and G418 solution were obtained from InvivoGen (San Diego, CA, USA). Hygromycin B solution was purchased from Enzo Life Science (Farmingdale, NY, USA). Anti-LANA (clone LN53), anti-Flag (clone M2) and anti-RNAPII (clone

CTD4H8) antibodies were purchased from Millipore-Sigma. Anti-CHD4 (D4B7), H3K27Ac (D5E4) and H3K4me1 (D1A9) antibodies were purchased from Cell Signaling Technology. Anti-ADNP (PA5-52286) antibody was purchased from Invitrogen. Streptavidin magnetic beads (Pierce) were purchased from Thermo Fisher Scientific™. All other chemicals were purchased from Millipore-Sigma (St. Louis, MO, USA) unless otherwise stated.

Cells, transfection and reagents. *i*SLK.219 cells were maintained in DMEM supplemented with 10% FBS, 1% penicillin-streptomycin-L-glutamine solution, 10 µg/ml puromycin, 400 µg/ml hygromycin B, and 250 µg/ml G418. *i*SLK cells were obtained from Dr. Don Ganem (Novartis Institute for Biomedical Research) and were maintained in DMEM supplemented with 10% FBS, 1% penicillin-streptomycin-L-glutamine solution and 10 µg/ml puromycin. BC-1 and BC-3 cell lines were obtained from ATCC (Manassas, VA, USA), expanded to obtain early passage stocks, and stored. The BCBL-1 cell line was also obtained from Dr. Ganem (University of California San Francisco). BC-1, BC-3, and BCBL-1 cell lines were cultured in RPMI 1640 medium supplemented with 15% FBS and 1% penicillin-streptomycin-L-glutamine solution. TREx BCBL-1 cells, which can induce Flagx3-HAx3-K-Rta in tetracycline inducible manner, was prepared before (28) were maintained in RPMI 1640 medium supplemented with 10% FBS, 1% penicillin-streptomycin-L-glutamine, 250 µg/ml hygromycin B, and 100 µg/ml blasticidin. Plasmids or siRNAs were transfected with Lipofectamine reagent (Thermo Fisher) or Lipofectamine RNAiMax reagent (Thermo Fisher) respectively according to the manufacturer's protocol.

Capture Hi-C. KSHV Capture Hi-C (CHi-C) was performed using a robust *in situ* CHi-C protocol with kitted reagents from Arima Genomics (San Diego, CA, USA) based on methods described for *in situ* Hi-C (89, 90), CHi-C (91-93), and as described previously (28). Briefly, cells were

crosslinked with 2% formaldehyde, lysed, and the genomic DNA digested with a cocktail of 4-cutter restriction endonucleases by incubation for 30 minutes at 37°C. The 5'-overhangs were then filled in and labeled with biotinylated dATP (biotin-14-dATP) by incorporation with Klenow fragment of DNA polymerase I (incubation for 45 minutes at 25°C). Ligation of the spatially proximal blunt-ended fragments was then performed with T4 DNA ligase (incubation for 15 minutes at 25°C). The formaldehyde crosslinks were reversed and the proximally-ligated, chimeric DNA products were purified with Agencourt AMPure XP paramagnetic beads (Beckman Coulter, Brea, CA, USA). The DNA was then fragmented to an average size of 400 bp with a Covaris E220 Focused-ultrasonicator (Covaris, Inc., Woburn, MA, USA) and size-selected to have a fragment size distribution of 200-600 bp with AMPure XP beads. The biotin-labeled ligation products were then selectively enriched by affinity capture with streptavidin magnetic beads (Arima Enrichment Beads). Subsequently, sequencing libraries were prepared with the Kapa HyperPrep Kit with Library Amplification Module (Roche, Basel, Switzerland) using a modified protocol for on-bead end repair, dA-tailing, and ligation of Illumina TruSeq sequencing adaptors.

The KSHV CHi-C library was then prepared from the Hi-C libraries as previously described (28). Briefly, target enrichment for KSHV genomic content was performed by solution hybridization with a custom-designed KSHV genomic capture probe library (xGen Lockdown Probes; Integrated DNA Technologies, Inc., Coralville, IA) (28) and subsequent capture of the hybridized targets with streptavidin beads (DynaBeads MyOne Streptavidin C1; Thermo Fisher) according to the manufacturer's standard protocol (Integrated DNA Technologies, Inc., Coralville, IA). The KSHV genome-enriched CHi-C library DNA was eluted and PCR enrichment (12 cycles) performed with high-fidelity KAPA HiFi HotStart DNA Polymerase (Kapa Biosystems,

512 Inc., Wilmington, MA). Libraries were multiplex sequenced (2 x 150bp, paired-end, ~50 million
513 mapped reads/mate pairs per sample) on an Illumina Hiseq 4000 sequencing system.

514

515 **Cleavage Under Targets and Release Using Nuclease (CUT&RUN).** CUT&RUN (70) was
516 performed essentially by following the online protocol established by Dr. Henikoff's lab with a
517 few modifications. Cells were washed with PBS and wash buffer [(20 mM HEPES-KOH pH 7.5,
518 150 mM NaCl, 0.5 mM Spermidine (Sigma, S2626) and proteinase inhibitor (Roche)]. After
519 removing the wash buffer, cells were captured on magnetic ConA beads (Polysciences, PA,
520 USA), in the presence of $CaCl_2$. Beads/cells complexes were washed with digitonin wash buffer
521 (0.02% digitonin, 20 mM HEPES-KOH pH 7.5, 150 mM NaCl, 0.5 mM Spermidine and 1x
522 proteinase inhibitor) 3 times, aliquoted, and incubated with specific antibodies in 250 μL volume.
523 The antibodies used in this study were: rabbit monoclonal anti-CHD4 (Cell Signaling, D4B7;
524 1:50); rat monoclonal anti-LANA (Millipore-Sigma, clone LN53; 1:50); rabbit anti-ADNP
525 polyclonal (Invitrogen, PA5-52286; 1:100); rabbit monoclonal anti-Acetylated Histone H3 lysine
526 27 (Cell Signaling, D5E4; 1:100), rabbit monoclonal anti-H3 monomethyl lysine 4 (Cell Signaling,
527 D1A9; 1:100), and rabbit monoclonal anti-H3 tri-methyl lysine 27 (Cell Signaling, C36B11;
528 1:100). After incubation, unbound antibody was removed by washing with digitonin wash buffer
529 3 times. Beads were then incubated with recombinant pAG-MNase, which was purified from
530 *E.coli* (**Supplementary Fig. 9**), in 250 μl digitonin wash buffer at 1.0 μg/mL final concentration
531 for one hour at 4°C with rotation. Unbound pAG-MNase was removed by washing with digitonin
532 wash buffer 3 times. Pre-chilled 2 mM $CaCl_2$ containing digitonin wash buffer (200 μL) was added
533 to beads and incubated on ice for 30 min. The pAG-MNase digestion was halted by the addition
534 of 200 μl 2× STOP solution (340 mM NaCl, 20 mM EDTA, 4 mM EGTA, 50 μg/ml RNase A, 50

μg/ml glycogen). The beads were incubated with shaking at 37°C for 10 min in a tube shaker at 500 rpm to release digested DNA fragments from the insoluble nuclear chromatin. The supernatant was collected after centrifugation (16,000 x g for 5 min at 4°C) and placed on a magnetic stand. DNA was extracted using the NucleoSpin kit (Takara Bio, Kusatsu, Shiga, Japan). Sequencing libraries were then prepared from 3 ng of CUT&RUN DNA with the Kapa HyperPrep Kit (Roche) according to the manufacturer's standard protocol. Libraries were multiplex sequenced (2 x 150bp, paired-end) on an Illumina HiSeq 4000 sequencing system to yield ~15 million mapped reads per sample. When necessary, *E. coli* genomic DNA read from a pAG-MNase incubation were used to normalize data as described previously (70).

Genomic data analysis.

The HiC-pro 2.11.1 pipeline (94) was used to align sequences from the Hi-C experiments against a combined assembly of reference genomes; the human hg19 (GRCh37) and KSHV (NC_009333.1). The reads were filtered for only uniquely mapped reads pairs by identifying intersection of each read-end, and the valid reads were provided by removing reads with self-circle, dangling-end, error, extra dangling-end, too short, too large, duplicated, and random breaks. The valid reads were stored as matrices and binned with resolution of 10000 bp. Iterative Correction and Eigenvector decomposition (ICE) normalization was used to treat the data with default parameters. The normalized counts were filtered to keep only the counts that mapped to both the human and KSHV genome by using Python with Pandas library. The results were visualized as dot plots using Matplotlib library.

556 The normalized counts were also used as input in subsequent analyses. In the analysis of KSHV
557 episome localization near centromeres, centromeres of human chromosome (hg19) were
558 downloaded from the UCSC Table Browser with a filter of 'centromere' as gap type. For each
559 chromosome, the sum of all counts was compared to both the sums of the counts in the regions
560 near the centromere at the 5' and 3' sides, both of which are 1% the size of the chromosome
561 (the values were first normalized as per 100,000 bp before the comparisons). The similarity of
562 CHi-C chimeric sequence reads among BC-1, BC-3, and BCBL-1 were performed as follows.
563 Genomic regions with normalized counts > 0 were extracted and then the intersect and union
564 regions were determined using Intervene v0.6.4 (95). The similarity percentage was calculated
565 based on the Jaccard similarity index.

566 FASTQ files for the capture Hi-C experiments were processed through the HiCUP (v0.7.4)
567 pipeline (96) using a combined human hg19 (GRCh37) and KSHV (NC_009333.1) genome.
568 Valid interaction products called by HiCUP were converted into Juicebox (97) input format (.hic
569 file), which stores the normalized and un-normalized contact matrices as a highly compressed
570 binary file, by using a series a scripts provided by HiCUP (hicup2homer) and HOMER
571 (makeTagDirectory and tagDir2hicFile) (98). Juicebox was utilized to facilitate adjustments of
572 resolution and normalization, intensity scaling, zooming, and addition of annotation tracks.

573 CUT&RUN sequence reads were aligned to the human hg38 reference genome and
574 reference KSHV genome sequence (Human herpesvirus 8 strain: GQ994935.1) with Bowtie2
575 v2.3.5.1 (99) and/or HISAT2 v2.1.0 (100). MACS2 (Model-based Analysis of ChIP-Seq)
576 v2.1.1.1.20160309 was used for detecting peaks (101) following the developer's manual. Peaks
577 and read alignments were visualized using the Integrated Genome Browser (IGB) (102).
578 Heatmaps and average profile plots were drawn from bed files created by MACS and bam files

using R package, ngsplot v2.63 (103). After subtracting the minimum value of average profile as background signal, relative average profile plot was drawn. Accumulation index was calculated as proportion of area under the curve.

Single cell RNA sequencing data analysis. Single cell data was analyzed with the Cell Ranger v2.1 pipeline (10x Genomics). The pipeline included alignment to the hg38 human reference genome and human herpesvirus 8 strain (GQ994935.1) reference genome, t-distributed stochastic neighbor embedding (tSNE), and K-means clustering. Read count matrices obtained from the pipeline were normalized using log normalization method with "Seurat" R package (104). To perform correlation analysis, the expression of the KSHV genes was summarized, log transformed and resulting values divided by 14 equal intervals to have more than 50 cells in each interval. The median value of gene expression was calculated for the cells in each interval. The median values were used to analyze and visualize the correlation of host cellular and viral gene expression.

Immunofluorescence staining analyses. *i*SLK cells latently infected with BAC16-Wt were seeded onto glass coverslips and transfected with pLenti-Flag-mCHD4-myc WT or pLenti-Flag-mCHD4-myc mutant using Lipofectamine 2000 reagent according to the manufacturer's protocol. pLenti-Flag-mCHD4-myc was obtained from a commercial source (Origene, MD, USA). Point mutations were inserted by synthesizing DNA fragments that contain intended mutations and replaced at SexAI-AgeI restriction sites with In-FusionHD (Takara Bio, Japan). At 24 hrs after transfection, 1 μg/ml of doxycycline and 20 ng/ml of 12-O-Tetradecanoylphorbol-13-acetate

(TPA) were added, and cells were cultured for a further 26 hrs in the presence of doxycycline and TPA. The cells were then fixed with 4% paraformaldehyde, permeabilized with 0.2% Triton X-100, and labeled with anti-RNAPII mouse monoclonal antibody (Millipore-Sigma, clone CTD4H8, 1:100) and anti-FLAG rabbit polyclonal antibody (Sigma, F7425, 1:100), followed by Alexa 555-anti mouse IgG and Alexa 647-anti rabbit IgG (Thermo Fisher). Nuclei were counterstained with 1μg/ml of Hoechst 33342 (Thermo Fisher). The labeled cells were observed with a Keyence BZ-X710 fluorescence microscope (Keyence, Osaka, Japan) with standard DAPI, GFP, TRITC and Cy5 filter sets (Chroma Technologies, Bellows Falls, VT, USA).

DNA-FISH combining with LANA immunostaining. BCBL-1 cells were washed with PBS twice and spotted on coverslips and fixed with 4% formaldehyde-PBS for 10 min at RT. Cells were subsequently incubated with PBS with 100 mM glycine to quench residual formaldehyde. Cells were treated with 0.1% Triton-X and 0.05% SDS with RNaseA for 15 min at 37°C. Coverslips were washed with PBS twice, 70% ethanol once, 85% ethanol once, and 100% ethanol once and dried completely. Cy5-conjugated CENPB-Cy5 PNA probe was obtained from a commercial source (PNA Bio, Thousand Oaks, CA, USA) and coverslips were incubated with hybridization buffer (200 nM PNA probe, 2xSSC, 20% Dextran, 1 mg/mL yeast tRNA, 60% formamide) on a glass slide on a heating plate at 57°C for 10 min and then 37°C for another 30 min. Utilization of PNA probes avoids harsh conditions often used for a larger DNA hybridization, which we found to produce unacceptable noise and not readily compatible with subsequent protein staining. The coverslip was washed with warmed 0.1% Tween 20 in PBS (57°C) in 6-well plates for 3 times and PBS once. Primary antibody was incubated for LANA staining in PBS with 1 mg/mL yeast tRNA. After washing with PBS 3 times, secondary antibody (Alexa 488-anti Rat IgG) was incubated in PBS with yeast tRNA for 1 h at 37°C. After washing three times with

PBS, the coverslips were mounted with antifade reagent (Thermo Fisher), and images were captured with a Keyence microscope.

3D Fluorescence microscopy and quantitative image analysis. Widefield 3D fluorescence imaging was performed on a Keyence BZ-X710 fluorescence microscope (Keyence, Osaka, Japan) equipped with live-cell environmental chamber. Cells fluorescently labeled as previously described were observed with standard DAPI, GFP, TRITC and Cy5 filter sets (Chroma Technologies, Bellows Falls, VT, USA). High resolution image stacks were acquired in each color channel using Keyence onboard software. Image stacks were converted to greyscale TIF images that were uniformly corrected for haze reduction, deblurring and contrast enhancement.

Image data were subsequently exported to the Volocity® Multi-Dimensional Imaging Platform (Quorum Technologies Inc., Ontario, Canada) for 3D visualization and quantitative analysis. For image-based cytometry measurements, individual cells within a given field of view were automatically identified and fluorescent objects and/or region of interest in the various color channels were quantified and tabulated. For qualitative assessment of LANA and centromere oligo probes for DNA-FISH, 3D image stacks were similarly compiled and displayed in 3D opacity mode using Volocity Visualization toolset. Reconstructed 3D images were used for distance-measurement analysis: briefly, fluorescent LANA dots (green) and DNA centromeres (purple) in individual cell nuclei were automatically identified in Volocity Quantitation. The minimum distance from each centromere to the nearest LANA dot could then be extracted from the statistical measurements and displayed as histograms for subsequent analysis.

Lentivirus production and transduction. For CHD4 knock-down experiments, the following shRNA sequences from Sigma pLKO.1 shRNA libraries were used: shRNA#1: CCTTACTAGAATTGGTGTTAT; shRNA#2: GCTGACACAGTTATTATCTAT. Lentiviruses generated from the CHD4-expressing lentivector, CHD4-targeting shRNAs, and non-targeting scramble shRNA (Addgene, #1864) were produced in 293T cells. The vectors were co-transfected with psPAX2 (Addgene, #12260) and pMD2.G (Addgene, #12259) into 293T cells using polyethylenimine (PEI). Supernatants were collected 48 and 72 hrs post-transfection. Cells were infected with lentiviruses in the presence of 8 μg/ml polybrene and subsequently incubated for 72 hrs to allow for protein expression or knock-down. To generate CHD4 knock-down cell lines, 293T cells were infected with lentivirus for 24 hrs. Cells were then cultured in selection medium containing 1 μg/ml puromycin for two weeks to obtain stable CHD4 knock-down cell lines.

Preparation of purified KSHV and *de novo* infection. *i*SLK.219 cells latently infected with recombinant KSHV were cultured in eight to ten 150 mm culture dishes until 80% confluent. For reactivation, cultures were re-fed with complete DMEM (without selection drugs) containing 0.3 mM sodium butyrate and 1 μg/ml doxycycline. The cells were further cultured for 5 days in the presence of sodium butyrate and doxycycline. The culture supernatant was centrifuged at 300 x g for 10 min, and then passed through a 0.8-μm filter to remove cellular debris, and then viral particles were concentrated by ultracentrifugation at 25,000 rpm for 2 hrs at 4 °C with a Beckman SW28 rotor. The viral precipitates were resuspended in 500 μl of DMEM along with the residual ~500 μl media in the centrifuge tube and stored at –80 °C until use. For *de novo* infection, CHD4-KD 293T cells were seeded at 4 x 10^5 cells/well in 6-well plates. After overnight

668 culture, viral stocks were added to the cultures and the infection was allowed to proceed for
669 24 hrs. Cells were monitored for GFP expression and RNA was purified using the RNeasy Mini
670 Kit (Qiagen, Venlo, Netherlands).

671

672 **Flow Cytometry.** 293T cells were transfected with 10 pmol CHD4 siRNA using Lipofectamine
673 RNAiMax reagent (Thermo Fisher) for 48 hrs. Cells were infected with r.219 virus for 96 hrs in
674 DMEM media containing 5% FBS. After that, cells were trypsinized and washed with PBS two
675 times followed by fixation with 2% PFA containing 1 mM EDTA for 10 minutes at 37 ºC. Cells
676 were then washed with PBS twice and resuspended in PBS containing 1 mM EDTA. Cells were
677 passed through a 0.45-µm strainer to obtain single cells. A BD "Fortessa" cytometer was used
678 for FACS analysis, and FlowJo software (Tree Star) was used for data analysis.

679

680 **Purification of recombinant protein.** *Spodoptera frugiperda* Sf9 cells (Millipore) were
681 maintained in Ex-Cell 420 medium (Sigma), and recombinant baculoviruses were generated with
682 the Bac to bac baculovirus expression system as previously described (20, 105). Transfer
683 plasmid, pFAST-BAC1 vector was modified by inserting a Flag tag at the N-terminus, and CHD4,
684 ORF57, p65, and Luciferase cDNAs were cloned into the CpoI (*Rsr*II) site. The cDNA of ADNP,
685 which also include C-terminal His tag was synthesized and cloned into *Bam*HI and *Pst*I restriction
686 enzyme sites by Gene assembly (NEB). Recombinant baculovirus bacmid DNA was transfected
687 into Sf9 cells by using polyethylenimine (Sigma), and recombinant viruses were subsequently
688 amplified twice. Expression of recombinant proteins was confirmed by immunoblotting with anti-
689 Flag monoclonal antibody (Sigma). Large-scale cultures of Sf9 cells (100 ml) were infected with

recombinant baculovirus at a multiplicity of infection (MOI) of 0.1 to 1.0, and cells were harvested 48 hrs after infection. Recombinant proteins were purified as described previously (106). The purity and amount of protein were measured by SDS-PAGE and Coomassie blue staining, using bovine serum albumin (BSA) as a standard.

***In vitro* interaction assays.** Baculoviruses expressing Flag-CHD4, His-ADNP, or Flag-LANA were co-infected in SF9 cells and purified by Flag tag capture in the presence of 500 mM NaCl and 10% glycerol. Purified complex was re-suspended in the binding buffer (20 mM HEPES [pH 7.9], 150 mM NaCl, 1 mM EDTA, 4 mM $MgCl_2$, 1 mM dithiothreitol, 0.02% NP-40, 10% glycerol supplemented with 1 mg/ml BSA, and 1× protease inhibitor cocktail) and the antibody was incubated at 1:100 dilution for 1 hrs at 4°C to form an immunocomplex. The immunocomplex was captured with 10 μL of protein A/G magnetic beads mixture. Beads were washed three times with binding buffer and subjected to SDS-PAGE after eluting proteins in sample buffer. The interaction was probed by immunoblotting with anti-CHD4, anti-ADNP, or anti-LANA antibody.

For RNA or DNA pull-down, a final concentration of 100 nM of each biotinylated RNA fragment (e.g. 1.3 μg for full length PAN RNA transcribed *in vitro* or 2.6 μg of dsDNA generated by PCR with 5'-biotinylated primer) and purified proteins (100 nM in final) was incubated in RNA-binding buffer (50 mM HEPES [pH 7.9], 150 mM KCl, 5% glycerol, 0.02% NP-40, 100 μg/mL yeast tRNA, 2 mM $MgCl_2$) supplemented with RNAse inhibitor in 40 μL reaction for 1 hrs at 4°C. Biotinylated RNA or dsDNA was captured with streptavidin conjugated magnetic beads, washed with binding buffer 3 times, and proteins were eluted in sample buffer. Precipitated proteins were

visualized by immunoblotting with either anti-Flag antibody (Sigma) or specific antibody as indicated in figure legends.

Construction of mini-Turbo KSHV BAC16. Recombinant KSHV was prepared by following a protocol for En passant mutagenesis with a two-step markerless red recombination technique (107). Briefly, the codon optimized mini-TurboID coding sequence (65), which also encodes the 3x Flag tag was first cloned into a pBS SK vector (Thermo Fisher, Waltham, MA USA). The pEPkan-S plasmid was used as a source of the kanamycin cassette, which includes the I-SceI restriction enzyme site at the 5'-end of the kanamycin coding region (107). The kanamycin cassette was amplified with primer pairs with homology arms and cloned into the mini-TurboID coding region at a unique restriction enzyme site. The resulting plasmid was used as a template for another round of PCR to prepare a transfer DNA fragment for markerless recombination with BAC16 (108). Recombinant BAC16 clones with insertion and also a deletion of the kanamycin cassette in the BAC16 genome were confirmed by colony PCR with appropriate primer pairs. Recombination junctions and adjacent genomic regions were amplified by PCR and the resulting PCR products were directly sequenced with the same primers to confirm in-frame insertion of the mini-TurboID cassette into the BAC16 DNA for mini-TurboID-ORF57 and -LANA. Insertion of PAN RNA MRE mutations was performed by using primer pairs that encode the intended mutations. Primer pairs were used to amplify the kanamycin cassette and recombination, deletion of kanamycin cassette, confirmation of mutations was performed as described above. The resulting recombinant BAC16 was confirmed by restriction enzyme digestions (*Hind*III and *Bgl*II) to determine if there were any large DNA deletions. Two independent BAC16 clones were generated for each mini-TurboID tagged recombinant KSHV virus as biological replicates and

735 one of the clones was used for protein ID. Entire BAC16 DNAs were subsequently sequenced
736 by NGS on an Illumina MiSeq System.

737 **Quantification of viral copy number.** Two hundred microliters of cell culture supernatant were
738 treated with DNase I (12 µg/ml) for 15 min at room temperature to degrade unencapsidated
739 DNA. This reaction was stopped by the addition of EDTA to 5 mM followed by heating at 70°C
740 for 15 min. Viral genomic DNA was purified using the QIAamp DNA Mini Kit according to the
741 manufacturer's protocol and eluted in 100 µl of buffer AE. Four microliters of the eluate were
742 used for real-time qPCR to determine viral copy number, as described previously (105).

743

744 **Real-time RT-PCR**. Total RNA was isolated using the Quick-RNA miniprep kit (Zymo Research,
745 Irvine, CA, USA). First-strand cDNA was synthesized using the High Capacity cDNA Reverse
746 Transcription Kit (Thermo Fisher, Waltham, MA USA). Gene expression was analyzed by
747 realtime qPCR using specific primers for KSHV ORFs designed by Fakhari and Dittmer (109).
748 We used 18S ribosomal RNA or GAPDH as an internal standard to normalize viral gene
749 expression.

750

751 **Western blotting.** Cells were lysed in IP lysis buffer (25 mM Tris-HCl pH 7.4, 150 mM NaCl, 1%
752 NP-40, 1 mM EDTA, 5% glycerol) containing protease inhibitors (Roche, Basel, Switzerland).
753 Total cell lysates (25 µg) were boiled in SDS-PAGE loading buffer and subjected to SDS-PAGE
754 and subsequently transferred to a polyvinylidene fluoride membrane (Millipore-Sigma, St. Louis,
755 MO, USA) using a semidry transfer apparatus (Bio-Rad, Hercules, CA, USA). The streptavidin-
756 HRP conjugate was used at 1:3000 dilution. Final dilution of the primary antibody was 1:3,000

for anti-Flag mouse antibody, 1:1,000 for anti-LANA rat antibody, anti-CHD4 rabbit, and anti-ADNP rabbit antibodies. Washing membranes and secondary antibody incubations were performed as described previously (105).

Affinity purification of biotinylated proteins. KSHV LANA-mTID cells were incubated with 100 μM D-biotin for 60 mins at 37ºC. To stop the reaction, cells were incubated at 4°C for 60 mins. Cells were washed with cold PBS three times followed by lysis with SUMO lysis buffer (Tris-Cl PH 6.8, 1% SDS and 10% glycerol). Lysates were immediately boiled for 10 min, and protein was quantified by Bradford assay (Bio-Rad). The biotinylation signal was confirmed by western blotting using Strep-HRP.

Affinity purification was performed with streptavidin-coated magnetic beads (Thermo-Fisher). Briefly, 150 μl magnetic beads/sample were pre-washed with RIPA lysis buffer (150 mM NaCl, 5 mM EDTA (pH 8), 50 mM Tris (pH 8), 1% NP-40, 0.5% sodium deoxycholate, 0.1% SDS) 3 times. A total of 3 mg of whole cell lysate was incubated with pre-washed streptavidin beads after diluting with RIPA buffer for 10 times, at room temperature for 1h with rotation. The beads were collected using a magnetic stand and washed three times with wash buffer according to the manufacturer's protocol. Finally, beads were resuspended in 200 μl of wash buffer and sent to UC Davis Proteomics core for on bead digestion and LC-MS/MS analysis.

MS sample preparation. Protein samples on magnetic beads were washed four times with 200 μl of 50 mM ammonium bicarbonate (AMBIC) with a twenty-minute shake time at 4°C in between each wash. Roughly 2.5 μg of trypsin was added to the beads and AMBIC and the samples were

digested overnight at 800 rpm shake speed. After overnight digestion, the supernatant was removed, and the beads were washed once with enough 50 mM AMBIC to cover them. After 20 minutes at a gentle shake the wash was removed and combined with the initial supernatant. The peptide extracts were reduced in volume by vacuum centrifugation and a small portion of the extract was used for fluorometric peptide quantification (Thermo Scientific Pierce). One microgram of sample based on the fluorometric peptide assay was loaded for each LC-MS analysis.

Digested peptides were analyzed by LC-MS/MS on a Thermo Scientific Q Exactive Orbitrap Mass spectrometer in conjunction with Proxeon Easy-nLC II HPLC (Thermo Scientific) and Proxeon nanospray source. The digested peptides were loaded on a 100 micron x 25 mm Magic C18 100Å 5U reverse phase trap where they were desalted online before being separated using a 75-micron x 150 mm Magic C18 200Å 3U reverse-phase column. Peptides were eluted using a 60-minute gradient with a flow rate of 300 μl/min. An MS survey scan was obtained for the m/z range 300-1600, MS/MS spectra were acquired using a top 15 method, where the top 15 ions in the MS spectra were subjected to HCD (High Energy Collisional Dissociation). An isolation mass window of 2.0 m/z was used for the precursor ion selection, and normalized collision energy of 27% was used for fragmentation. A fifteen second duration was used for the dynamic exclusion.

MS/MS analysis. Tandem mass spectra were extracted and charge state deconvoluted by Proteome Discoverer (Thermo Scientific). All MS/MS samples were analyzed using X! Tandem (The GPM, thegpm.org; version X! Tandem Alanine (2017.2.1.4)). X! Tandem was set up to search the Human and Kaposi's Sarcoma Herpes virus database (149182 entries) assuming the

digestion enzyme trypsin. X! Tandem was searched with a fragment ion mass tolerance of 20 PPM and a parent ion tolerance of 20 PPM. Carbamidomethyl of cysteine and selenocysteine was specified in X! Tandem as a fixed modification. Glu->pyro-Glu of the N-terminus, ammonia-loss of the N-terminus, gln->pyro-Glu of the N-terminus, deamination of asparagine and glutamine, oxidation of methionine and tryptophan and dioxidation of methionine and tryptophan were specified in X! Tandem as variable modifications.

Scaffold (version Scaffold_4.8.4, Proteome Software Inc., Portland, OR) was used to validate MS/MS-based peptide and protein identifications. Peptide identifications were accepted if they could be established at greater than 98.0% probability by the Scaffold Local FDR algorithm. Peptide identifications were also required to exceed specific database search engine thresholds. Protein identifications were accepted if they could be established at greater than 5.0% probability to achieve an FDR less than 5.0% and contained at least 2 identified peptides. Protein probabilities were assigned by the Protein Prophet algorithm (110). Proteins that contained similar peptides and could not be differentiated based on MS/MS analysis alone were grouped to satisfy the principles of parsimony. Proteins sharing significant peptide evidence were grouped into clusters.

Pathway analysis. The proteins identified to be interacting with ORF57 were used for gene ontology analysis. The top gene ontology processes were enriched by the Metascape web-based platform, and the Metascape software was used for gene ontology analysis (111).

Statistical analysis. Results are shown as mean ± SD from at least three independent experiments. Data were analyzed using unpaired Student's t test, or ANOVA followed by Tukey's HSD test. A value of $p<0.05$ was considered statistically significant.

Code availability. All custom codes used to analyze data and generate figures are available upon request.

Data availability. Data can be accessed via the Source Data files and Supplementary tables. The genomic data discussed in this publication have been deposited in NCBI's GEO Database under unified Super Series GSE163695 with subseries GSE163098 for CUT&RUN and GSE163694 for CHi-C.

Acknowledgement. This research was supported by public health grants from the National Cancer Institute (CA225266, CA232845), the National Institute of Dental and Craniofacial (DE025985), and the National Institute of Allergy and Infectious Disease (AI147207) to Y.I. The Genomics Shared Resource is supported by the UC Davis Comprehensive Cancer Center Support Grant (CCSG) awarded by the National Cancer Institute (NCI P30CA093373).

Author Contributions.

A.K., Y.L., M.C., and Y.I. designed and performed experiments, analyzed data and prepared figures. Y.Y., C.C., R.R.D., K.N., and A.M. ran genomic pipelines, performed statistical analyses,

and visualized genomic data sets. M.S. prepared enzyme digested protein samples and performed proteomics data analyses. R.R.D. and C.G.T. prepared sequencing libraries and performed initial bioinformatics analyses. K.I.N and R.R.D. prepared single cell transcriptomics libraries, and A.M. wrote custom codes and analyzed single-cell sequence data sets. A.K., Y.L., K.W., C.I., and Y.I. prepared BAC stable cell lines, and performed molecular and biochemical studies. YI generated recombinant BACs. F.C. and K.I.N. prepared slides and performed imaging analyses. V.M., M.S., and Z.M.Z. contributed key reagents. A.K, Y.L., Y.Y., C.C., M.S., F.C., R.R.D., C.G.T., K.N., K.I.N., V.M., Z.M.Z. and Y.I. analyzed corresponding data sets. Y.I. wrote the manuscript and all authors edited the manuscript.

Competing financial interests.

The authors have declared that no conflicts of interest exist.

Materials & Correspondence.

Correspondence and request for materials should be addressed to M.C. (e-mail: mcampbell@ucdavis.edu) or Y.I. (email: yizumiya@ucdavis.edu).

Figure legends

Fig. 1 KSHV episome-tethering sites in KSHV positive cell lines. (a) Schematic workflow for Capture-HiC (CHi-C). (b) KSHV episome-docking sites on host cell chromosomes. CHi-C chimeric DNA ligation products composed of sequences derived from the KSHV and human genomes were mapped in three naturally-infected PEL cells. For BCBL-1 cells, three biological replicates were performed with nearly identical results (similarity 0.95). M, mitochondrial chromosome. ICE-corrected profiles depicting sums of filtered read counts binned at 10 kb resolution are shown. **(c) Selected chromosome 1 in zoomed view.** Chromosome 1 dot plots were depicted, which displays enrichment of sequence reads near the centromere. Red arrows indicate the position of the centromere. Extended panels for all other individual chromosome for three cell lines are presented in Supplementary Fig. 1a-c. **(d) KSHV episomes preferentially localize near the centromere.** KSHV episome contacts were calculated in BCBL-1 cells for sequence reads in 1% (length of the respective chromosome) of the 5'-and 3'-centromere and compared with the average of the total chromosome read count. **(e) LANA protein locates near the centromere.** DNA-FISH was used to visualize the location of the centromere (red) and KSHV episomes were indirectly visualized by staining LANA dots (Green) in BCBL-1 cells. The centromere and LANA were probed using a Cenp probe and anti-LANA antibody respectively with IFA. The two signals were frequently co-localized, and 3D view and their image analyses are presented in Supplementary Fig. 2. **(f) Jaccard statistics and Venn diagram.** Venn diagram shows percent similarity of KSHV episome-tethering positions among BC-1, BC-3 and BCBL-1 cells.

Fig. 2 LANA interacts with the ChAHP complex. (a) A schematic diagram of preparation of recombinant KSHV infected *i*SLK cells. A mini-TurboID (mTID) was fused to the N-terminus of the LANA open reading frame to generate KSHV LANA-mTID. KSHV LANA-mTID was transfected into *i*SLK cells followed by production of viral particles by stimulating cells with doxycycline (1 μg/ml) and sodium butyrate (3 mM) for 5 days. Virus was used to infect *i*SLK cells and cells were selected with hygromycin (1 mg/ml) to obtain an *i*SLK-LANA mTID stable cell line. **(b) Experimental design for preparing samples for protein ID.** *i*SLK-LANA mTID cells were left un-incubated (-) or incubated (+) with D-Biotin (500 μM) for 1 hr. Unincubated (-) cells were used as control samples. Each protein ID was performed in three biological replicates. **(c) Volcano plot depicting proteins in close proximity to LANA.** The volcano plot represents proteins identified in close proximity to LANA. Proteins with an abundance Log2 FC of greater than or equal to 1 and p-value less than 0.05 were selected and are shown by blue box. T-test was used for calculating the p-value. Purple color; ChAHP components. Red color; previously identified proteins as LANA interacting proteins. **(d) LANA interacts with CHD4 and ADNP *in vitro*.** LANA, CHD4 and ADNP complex, which consists of Flag-LANA (gold arrow), Flag-CHD4 (blue arrow), and His-ADNP (green arrow) was prepared by co-infected three recombinant baculoviruses, and the protein complex was isolated in the presence of 500 mM NaCl and 10% glycerol with affinity purification. The authenticity of respective protein band was confirmed by immunoblotting with specific antibodies. Coomassie staining is shown. An equimolar amount (100 nM) of the three proteins were incubated in binding buffer and immunoprecipitated with the specific antibodies of one another. Ten percent of the reaction before immunoprecipitation was shown as controls. W.B: Western Blotting, Co-IP: Co-immunoprecipitation. **(e) CHD4 interaction site on LANA.** Purified GST-tagged LANA deletions, Flag-tagged luciferase and

Flag-tagged CHD4 were prepared from recombinant baculovirus infected Sf9 cells. An equal amount (1 μg) of each LANA deletion protein was incubated with full length Flag-tagged luciferase (1 μg) or Flag-tagged CHD4 (1 μg) in binding buffer and interaction was probed with anti-Flag antibody. LANA deletion proteins used for this GST-pull down assay are presented in Supplementary Fig. 4. **(f) LANA co-localizes with CHD4 in BCBL-1.** CHD4 and LANA were probed with anti-CHD4 rabbit monoclonal antibody and anti-LANA rat monoclonal antibody, respectively. Images were taken with Keyence fluorescence microscopy. Scale bar (20 μm) is shown.

Fig. 3 Association of ChAHP complex binding with KSHV episome-tethering sites. (a) CUT&RUN analysis for LANA, ADNP, CHD4 and H3K27Ac. The indicated antibodies were used for CUT&RUN in BCBL-1 cells. CUT&RUN peaks were visualized with Integrative Genomics Viewer (IGV) and a snapshot of one of the major binding sites (IRF4 super enhancer region) is shown. The number on the left-hand side denotes the height of the peak (e.g., read depth) and the number along the top denotes the positions on chromosome 6. **(b) Heatmaps for co-occupancies of LANA with ADNP, CHD4 and H3K27Ac on chromosomes.** Heatmap (middle) and average profile (bottom) showing correlation of LANA enrichment (by color intensity and region) with ADNP, CHD4, and H3K27Ac occupancies. Average profile plot summarizing the heatmap (bottom). The lighter green shade represents the standard error (SEM) on the average profile plot. Color keys are shown on the each heatmap (top). **(c) Heatmaps for correlation of CHi-C with CUT&RUN signals.** The association between CHi-C chimeric reads and LANA, CHD4, ADNP and H3K4me1 CUT&RUN peaks were depicted as heatmap and average profile plot. **(d) Accumulation index around CHD4 binding sites.** The accumulation

of CHD4 is displayed as a proportion of area under the curve of the relative average profile. Association between distance from CHD4 summit peak and relative chimeric sequence counts is shown as a bar chart.

Fig. 4 LANA, CHD4 and ADNP colocalize on the KSHV genome. **(a) CUT&RUN analysis.** The indicated antibodies were used for CUT&RUN in BCBL-1 cells and sequence reads were mapped to the KSHV genome. An IGV snapshot and KSHV genome map are shown. The number on the left-hand side denotes the height of the peak (e.g., read depth), the number along the top denotes the position on KSHV genome in kilobase (kb) and the number on the right-hand side indicated by arrow denote the height of the peak on terminal repeat region (TR). Selected region is zoomed in to show Ori-RNA and PAN RNA region. Primer used in Fig. 4b is also shown with red arrows and number show the exact location of the amplified region by the primers. (**b**) **Regulation of CHD4 on the KSHV episome during reactivation.** TREx-BCBL-1 cells were reactivated with doxycycline (1 μg/ml) and sodium butyrate (3 mM) for 24 hrs. CUT&RUN was performed on un-reactivated (latency) and reactivated cells for CHD4. CHD4 binding on the PAN RNA promoter region **(red arrow in Fig. 4a, right panel)** was calculated relative to the input sample (n=3, two biological replicates are shown). **(c) Detachment of KSHV episomes by reactivation.** BCBL-1 cells were reactivated with doxycycline (1 μg/ml) and TPA (20 nM) for 24 hrs. Chimeric sequence reads for un-reactivated (latency) and reactivated cells were mapped to the host chromosomes and visualized by Juicebox. Relative KSHV episome tethering during reactivation for the selected region on chromosome 1 was calculated by subtracting relative chimeric sequence reads in latency from relative chimeric sequence reads during reactivation. Blue and red dots indicate decreased and increased chimeric sequence reads respectively.

Fig. 5 CHD4 is both an RNA and DNA binding protein. (a) A schematic diagram of recombinant KSHVs. Mini-TurboID is fused to the N-terminus of ORF57 open reading frame and the ORF57 binding site (MRE) of PAN RNA was mutated as shown. **(b) Immunoblotting.** Recombinant KSHV infected *i*SLK cells (TID-57 PAN-Wt and -MRE) were either untreated or induced for reactivation with doxycycline (1 µg/ml) and TPA (20 nM) for 24 hrs. Blots were probed with either anti-Flag antibody (for mini-TurboID-ORF57) or Streptavidin-HRP (for biotinylated proteins). **(c) Venn diagram.** The Venn diagram indicates the number of identified proteins with a P value less than 0.05. Each protein ID was performed in three biological replicates. **(d) PAN RNA-mediated interacting proteins with ORF57.** The proteins found enriched in PAN RNA-WT samples are shown. The entire list of proteins and peptide counts are presented in Supplementary Table 2. **(e) siRNA screening with KSHV reactivation as readout.** Recombinant KSHV reactivation, which encodes RFP under control of the PAN RNA promoter, was used to screen the effects of KSHV reactivation. RFP signal intensity was measured with Image J, and the GFP signal was used as internal controls. Three randomly selected fields in the middle of each well were quantified and the average intensity was plotted. **(f) Recombinant proteins and synthesized PAN RNAs.** Recombinant Flag-tagged proteins were expressed with baculovirus and purified with Flag-agarose beads. Coomassie staining of Flag-CHD4, Flag-NF-kB (p65), and Flag-luciferase used for pull-down studies are shown. **(g) Schematic for *in vitro* interaction assay performed in Fig. 5 (h-j). (h) CHD4 binds RNAs in a sequence-independent manner.** RNA pull-down was performed with the indicated biotinylated PAN RNA deletions, mutation (MRE), and irrelevant RNA (luciferase mRNA), and interaction was probed by immunoblotting with anti-Flag antibody. Beads alone (No RNA) was used for background

975 control. **(i)** RNA pull down was performed with indicated biotinylated RNAs, and p65 and
976 Luciferase (Luc) were visualized by using anti-Flag antibody. **(j) PAN RNA competes with**
977 **CHD4 DNA binding.** Pull-down analyses with biotinylated ssRNA or dsDNA was performed.
978 CHD4 (100 nM) was incubated with biotinylated RNA (100 nM) or biotinylated dsDNA (100 nM)
979 in 40 µL binding buffer. Increasing amounts of non-biotinylated PAN RNA at 1:1, 1:10, and 1:20
980 (dsDNA vs. ssRNA) were also incubated, and precipitated CHD4 protein in the pull-down was
981 probed with anti-Flag antibody. Flow-through and 10% of the input reaction before pull-down
982 were used as control.

983

984 **Fig. 6 CHD4 is important for latency maintenance and establishment. (a) CHD4**
985 **overexpression, knockdown and complementation.** The *i*SLK.219 cell line was transfected
986 with empty vector (Vec) or mouse CHD4 cDNA or human CHD4 shRNA, or CHD4 shRNA and
987 mouse CHD4 cDNA for 48 hrs followed by KSHV reactivation with doxycycline (1 µg/ml) for 5
988 days. Encapsidated KSHV genomes in the culture supernatants were measured by qPCR to
989 assess effects of CHD4 overexpression or knockdown on KSHV reactivation. **(b) CHD4 ATPase**
990 **activity is important for prevention of nuclear aggregate formation.** *i*SLK cells latently
991 infected with BAC16-Wt was transfected with Flag-tagged mouse wild type CHD4, or an ATPase
992 domain mutant was transfected and stained with anti-Flag. Transcriptional factory formation was
993 assessed by staining RNAII. The percentage of aggregate formation in Flag-positive cells was
994 measured and plotted. Three biological replicates were performed, and 50 cells were counted in
995 each of the three biological replicates. **(c) CHD4 ATPase activity is important for inhibiting**
996 **viral gene expression during reactivation.** *i*SLK.219 cells were transduced with an equal
997 amount of CHD4 wild type (wt) and CHD4 mutant (mt) lentivirus for 2 days. Cells were

reactivated with doxycycline (1 μg/ml) for 2 days and ORF50 and ORF57 gene expression was quantified by RT-qPCR. Untreated cells were used for calculating the relative expression of ORF50 and ORF57. GAPDH was used as a negative control. *p<0.05, ***p<0.001 (comparing with CHD4 Wt). **(d-e) Single cell sequencing.** *i*SLK.219 cells were reactivated by induction of K-Rta expression from doxycycline inducible promoter for 24 hrs. Single-cell sequencing was performed with the 10x Genomics platform. A cell suspension was prepared followed by cell partitioning and 3' cDNA synthesis on the Chromium Controller and dual-index library preparation with 10x Genomics kitted reagents. **(d) tSNE**. tSNE was applied to separate cell clusters and KSHV gene (**d, left panel**) and CHD4 (**d, right panel**) expressing cells were marked. **(e) Negative correlation between CHD4 and viral gene expression.** Cells were divided into groups based on the amount of KSHV transcripts. A table and distribution of cell numbers and amount of KSHV transcripts are shown in Supplementary Fig. 6a-b. Intervals used to separate cell groups are also listed in Supplementary Fig. 6b. A correlation was established based on CHD4 expression in different groups of KSHV transcripts. **(f-h) CHD4 knockdown and KSHV lytic gene expression during *de novo* infection.** 293T cells were transduced with scramble shRNA (shScrm) or shCHD4 and stably selected with antibiotic. Immunoblot (**f**) and RT-qPCR (**g**) analysis of CHD4 in the 293T stable cell lines are shown. 293T stable cells were infected with rKSHV.219 for 24 hrs and total RNA was harvested at the indicated time points. **(h)** K-Rta and PAN RNA, was measured by RT-qPCR and normalized to GAPDH. *p<0.05, **p<0.01 (comparing with shScrm). **(i) Flow cytometry**. 293T cells were transfected with control siRNA (siC) or CHD4 siRNA (siCHD4) for 48 hrs followed by infection with rKSHV.219 virus for 96 hrs. Flow cytometry analysis was performed to calculate the number of GFP- and RFP-positive cells in siC and siCHD4 knockdown cells. **(j) KSHV latency model with ChAHP.** KSHV episomes

tether at epigenetically active regions with the ChAHP complex, and TR-loaded LANA/ChAHP prevents robust viral lncRNA expression. The action of robust lncRNA expression in lytic KSHV infection functions as an enhancer for viral ORFs that are physically neighboring with lncRNA genomic regions. Stimulation of K-Rta, in part by decreased CHD4 expression, triggers robust PAN RNA expression in the presence of ORF57, which competes with CHD4 DNA binding to enhance KSHV reactivation and detach KSHV episomes from CHD4-enriched host chromosome regions.

Reference

1. **Chang Y, Cesarman E, Pessin MS, Lee F, Culpepper J, Knowles DM, Moore PS.** 1994. Identification of herpesvirus-like DNA sequences in AIDS-associated Kaposi's sarcoma. Science **266:**1865-1869.
2. **Ganem D.** 2010. KSHV and the pathogenesis of Kaposi sarcoma: listening to human biology and medicine. J Clin Invest **120:**939-949.
3. **Mesri EA, Cesarman E, Boshoff C.** 2010. Kaposi's sarcoma and its associated herpesvirus. Nat Rev Cancer **10:**707-719.
4. **Schulz TF.** 2006. The pleiotropic effects of Kaposi's sarcoma herpesvirus. J Pathol **208:**187-198.
5. **Wong EL, Damania B.** 2005. Linking KSHV to human cancer. Curr Oncol Rep **7:**349-356.
6. **Cesarman E, Moore PS, Rao PH, Inghirami G, Knowles DM, Chang Y.** 1995. In vitro establishment and characterization of two acquired immunodeficiency syndrome-related lymphoma cell lines (BC-1 and BC-2) containing Kaposi's sarcoma-associated herpesvirus-like (KSHV) DNA sequences. Blood **86:**2708-2714.
7. **Cesarman E, Knowles DM.** 1999. The role of Kaposi's sarcoma-associated herpesvirus (KSHV/HHV-8) in lymphoproliferative diseases. Semin Cancer Biol **9:**165-174.
8. **Kedes DH, Lagunoff M, Renne R, Ganem D.** 1997. Identification of the gene encoding the major latency-associated nuclear antigen of the Kaposi's sarcoma-associated herpesvirus. J Clin Invest **100:**2606-2610.
9. **Nakamura H, Lu M, Gwack Y, Souvlis J, Zeichner SL, Jung JU.** 2003. Global changes in Kaposi's sarcoma-associated virus gene expression patterns following expression of a tetracycline-inducible Rta transactivator. J Virol **77:**4205-4220.
10. **Lu M, Suen J, Frias C, Pfeiffer R, Tsai MH, Chuang E, Zeichner SL.** 2004. Dissection of the Kaposi's sarcoma-associated herpesvirus gene expression program by using the viral DNA replication inhibitor cidofovir. J Virol **78:**13637-13652.
11. **Ellison TJ, Izumiya Y, Izumiya C, Luciw PA, Kung HJ.** 2009. A comprehensive analysis of recruitment and transactivation potential of K-Rta and K-bZIP during reactivation of Kaposi's sarcoma-associated herpesvirus. Virology **387:**76-88.
12. **Ballestas ME, Kaye KM.** 2011. The latency-associated nuclear antigen, a multifunctional protein central to Kaposi's sarcoma-associated herpesvirus latency. Future Microbiol **6:**1399-1413.
13. **Stedman W, Deng Z, Lu F, Lieberman PM.** 2004. ORC, MCM, and histone hyperacetylation at the Kaposi's sarcoma-associated herpesvirus latent replication origin. J Virol **78:**12566-12575.
14. **Verma SC, Choudhuri T, Kaul R, Robertson ES.** 2006. Latency-associated nuclear antigen (LANA) of Kaposi's sarcoma-associated herpesvirus interacts with origin recognition complexes at the LANA binding sequence within the terminal repeats. J Virol **80:**2243-2256.
15. **Hu J, Garber AC, Renne R.** 2002. The latency-associated nuclear antigen of Kaposi's sarcoma-associated herpesvirus supports latent DNA replication in dividing cells. J Virol **76:**11677-11687.
16. **Barbera AJ, Chodaparambil JV, Kelley-Clarke B, Joukov V, Walter JC, Luger K, Kaye KM.** 2006. The nucleosomal surface as a docking station for Kaposi's sarcoma herpesvirus LANA. Science **311:**856-861.
17. **Piolot T, Tramier M, Coppey M, Nicolas JC, Marechal V.** 2001. Close but distinct regions of human herpesvirus 8 latency-associated nuclear antigen 1 are responsible for nuclear targeting and binding to human mitotic chromosomes. J Virol **75:**3948-3959.
18. **Ottinger M, Christalla T, Nathan K, Brinkmann MM, Viejo-Borbolla A, Schulz TF.** 2006. Kaposi's sarcoma-associated herpesvirus LANA-1 interacts with the short variant of BRD4 and releases cells from a BRD4- and BRD2/RING3-induced G1 cell cycle arrest. J Virol **80:**10772-10786.
19. **Matsumura S, Persson LM, Wong L, Wilson AC.** 2010. The latency-associated nuclear antigen interacts with MeCP2 and nucleosomes through separate domains. J Virol **84:**2318-2330.

20. **Kim KY, Huerta SB, Izumiya C, Wang DH, Martinez A, Shevchenko B, Kung HJ, Campbell M, Izumiya Y.** 2013. Kaposi's sarcoma-associated herpesvirus (KSHV) latency-associated nuclear antigen regulates the KSHV epigenome by association with the histone demethylase KDM3A. J Virol **87:**6782-6793.
21. **Wang N, Wu R, Tang D, Kang R.** 2021. The BET family in immunity and disease. Signal Transduct Target Ther **6:**23.
22. **You J, Srinivasan V, Denis GV, Harrington WJ, Jr., Ballestas ME, Kaye KM, Howley PM.** 2006. Kaposi's sarcoma-associated herpesvirus latency-associated nuclear antigen interacts with bromodomain protein Brd4 on host mitotic chromosomes. J Virol **80:**8909-8919.
23. **Hu J, Yang Y, Turner PC, Jain V, McIntyre LM, Renne R.** 2014. LANA binds to multiple active viral and cellular promoters and associates with the H3K4methyltransferase hSET1 complex. PLoS Pathog **10:**e1004240.
24. **Lagunoff M, Ganem D.** 1997. The structure and coding organization of the genomic termini of Kaposi's sarcoma-associated herpesvirus. Virology **236:**147-154.
25. **Domsic JF, Chen HS, Lu F, Marmorstein R, Lieberman PM.** 2013. Molecular basis for oligomeric-DNA binding and episome maintenance by KSHV LANA. PLoS Pathog **9:**e1003672.
26. **Correia B, Cerqueira SA, Beauchemin C, Pires de Miranda M, Li S, Ponnusamy R, Rodrigues L, Schneider TR, Carrondo MA, Kaye KM, Simas JP, McVey CE.** 2013. Crystal structure of the gamma-2 herpesvirus LANA DNA binding domain identifies charged surface residues which impact viral latency. PLoS Pathog **9:**e1003673.
27. **Kim J, Dean A.** 2021. Enhancers navigate the three-dimensional genome to direct cell fate decisions. Curr Opin Struct Biol **71:**101-109.
28. **Campbell M, Watanabe T, Nakano K, Davis RR, Lyu Y, Tepper CG, Durbin-Johnson B, Fujimuro M, Izumiya Y.** 2018. KSHV episomes reveal dynamic chromatin loop formation with domain-specific gene regulation. Nat Commun **9:**49.
29. **Chen CP, Lyu Y, Chuang F, Nakano K, Izumiya C, Jin D, Campbell M, Izumiya Y.** 2017. Kaposi's Sarcoma-Associated Herpesvirus Hijacks RNA Polymerase II To Create a Viral Transcriptional Factory. J Virol **91**.
30. **Naik NG, Nguyen TH, Roberts L, Fischer LT, Glickman K, Golas G, Papp B, Toth Z.** 2020. Epigenetic factor siRNA screen during primary KSHV infection identifies novel host restriction factors for the lytic cycle of KSHV. PLoS Pathog **16:**e1008268.
31. **Strahan RC, McDowell-Sargent M, Uppal T, Purushothaman P, Verma SC.** 2017. KSHV encoded ORF59 modulates histone arginine methylation of the viral genome to promote viral reactivation. PLoS Pathog **13:**e1006482.
32. **Rossetto CC, Pari G.** 2012. KSHV PAN RNA associates with demethylases UTX and JMJD3 to activate lytic replication through a physical interaction with the virus genome. PLoS Pathog **8:**e1002680.
33. **Gunther T, Frohlich J, Herrde C, Ohno S, Burkhardt L, Adler H, Grundhoff A.** 2019. A comparative epigenome analysis of gammaherpesviruses suggests cis-acting sequence features as critical mediators of rapid polycomb recruitment. PLoS Pathog **15:**e1007838.
34. **Toth Z, Maglinte DT, Lee SH, Lee HR, Wong LY, Brulois KF, Lee S, Buckley JD, Laird PW, Marquez VE, Jung JU.** 2010. Epigenetic analysis of KSHV latent and lytic genomes. PLoS Pathog **6:**e1001013.
35. **Gunther T, Grundhoff A.** 2010. The epigenetic landscape of latent Kaposi sarcoma-associated herpesvirus genomes. PLoS Pathog **6:**e1000935.
36. **Clarkson CT, Deeks EA, Samarista R, Mamayusupova H, Zhurkin VB, Teif VB.** 2019. CTCF-dependent chromatin boundaries formed by asymmetric nucleosome arrays with decreased linker length. Nucleic Acids Res **47:**11181-11196.
37. **Barisic D, Stadler MB, Iurlaro M, Schubeler D.** 2019. Mammalian ISWI and SWI/SNF selectively mediate binding of distinct transcription factors. Nature **569:**136-140.
38. **Goodman JV, Yamada T, Yang Y, Kong L, Wu DY, Zhao G, Gabel HW, Bonni A.** 2020. The chromatin remodeling enzyme Chd4 regulates genome architecture in the mouse brain. Nat Commun **11:**3419.

39. **Ostapcuk V, Mohn F, Carl SH, Basters A, Hess D, Iesmantavicius V, Lampersberger L, Flemr M, Pandey A, Thoma NH, Betschinger J, Buhler M.** 2018. Activity-dependent neuroprotective protein recruits HP1 and CHD4 to control lineage-specifying genes. Nature **557:**739-743.
40. **Sun X, Yu W, Li L, Sun Y.** 2020. ADNP Controls Gene Expression Through Local Chromatin Architecture by Association With BRG1 and CHD4. Front Cell Dev Biol **8:**553.
41. **Arends T, Dege C, Bortnick A, Danhorn T, Knapp JR, Jia H, Harmacek L, Fleenor CJ, Straign D, Walton K, Leach SM, Feeney AJ, Murre C, O'Connor BP, Hagman JR.** 2019. CHD4 is essential for transcriptional repression and lineage progression in B lymphopoiesis. Proc Natl Acad Sci U S A **116:**10927-10936.
42. **Farnung L, Ochmann M, Cramer P.** 2020. Nucleosome-CHD4 chromatin remodeler structure maps human disease mutations. Elife **9**.
43. **Kaaij LJT, Mohn F, van der Weide RH, de Wit E, Buhler M.** 2019. The ChAHP Complex Counteracts Chromatin Looping at CTCF Sites that Emerged from SINE Expansions in Mouse. Cell **178:**1437-1451 e1414.
44. **Zhao H, Han Z, Liu X, Gu J, Tang F, Wei G, Jin Y.** 2017. The chromatin remodeler Chd4 maintains embryonic stem cell identity by controlling pluripotency- and differentiation-associated genes. J Biol Chem **292:**8507-8519.
45. **Wang HC, Chou CL, Yang CC, Huang WL, Hsu YC, Luo CW, Chen TJ, Li CF, Pan MR.** 2019. Over-Expression of CHD4 Is an Independent Biomarker of Poor Prognosis in Patients with Rectal Cancers Receiving Concurrent Chemoradiotherapy. Int J Mol Sci **20**.
46. **Xia L, Huang W, Bellani M, Seidman MM, Wu K, Fan D, Nie Y, Cai Y, Zhang YW, Yu LR, Li H, Zahnow CA, Xie W, Chiu Yen RW, Rassool FV, Baylin SB.** 2017. CHD4 Has Oncogenic Functions in Initiating and Maintaining Epigenetic Suppression of Multiple Tumor Suppressor Genes. Cancer Cell **31:**653-668 e657.
47. **Kovac K, Sauer A, Macinkovic I, Awe S, Finkernagel F, Hoffmeister H, Fuchs A, Muller R, Rathke C, Langst G, Brehm A.** 2018. Tumour-associated missense mutations in the dMi-2 ATPase alters nucleosome remodelling properties in a mutation-specific manner. Nat Commun **9:**2112.
48. **Weiss K, Terhal PA, Cohen L, Bruccoleri M, Irving M, Martinez AF, Rosenfeld JA, Machol K, Yang Y, Liu P, Walkiewicz M, Beuten J, Gomez-Ospina N, Haude K, Fong CT, Enns GM, Bernstein JA, Fan J, Gotway G, Ghorbani M, Study DDD, van Gassen K, Monroe GR, van Haaften G, Basel-Vanagaite L, Yang XJ, Campeau PM, Muenke M.** 2016. De Novo Mutations in CHD4, an ATP-Dependent Chromatin Remodeler Gene, Cause an Intellectual Disability Syndrome with Distinctive Dysmorphisms. Am J Hum Genet **99:**934-941.
49. **Sartorelli V, Lauberth SM.** 2020. Enhancer RNAs are an important regulatory layer of the epigenome. Nat Struct Mol Biol **27:**521-528.
50. **Bose DA, Donahue G, Reinberg D, Shiekhattar R, Bonasio R, Berger SL.** 2017. RNA Binding to CBP Stimulates Histone Acetylation and Transcription. Cell **168:**135-149 e122.
51. **Hah N, Murakami S, Nagari A, Danko CG, Kraus WL.** 2013. Enhancer transcripts mark active estrogen receptor binding sites. Genome Res **23:**1210-1223.
52. **Rahnamoun H, Lee J, Sun Z, Lu H, Ramsey KM, Komives EA, Lauberth SM.** 2018. RNAs interact with BRD4 to promote enhanced chromatin engagement and transcription activation. Nat Struct Mol Biol **25:**687-697.
53. **Morf J, Basu S, Amaral PP.** 2020. RNA, Genome Output and Input. Front Genet **11:**589413.
54. **Song MJ, Brown HJ, Wu TT, Sun R.** 2001. Transcription activation of polyadenylated nuclear rna by rta in human herpesvirus 8/Kaposi's sarcoma-associated herpesvirus. J Virol **75:**3129-3140.
55. **Sun R, Lin SF, Gradoville L, Miller G.** 1996. Polyadenylylated nuclear RNA encoded by Kaposi sarcoma-associated herpesvirus. Proc Natl Acad Sci U S A **93:**11883-11888.
56. **Conrad NK, Steitz JA.** 2005. A Kaposi's sarcoma virus RNA element that increases the nuclear abundance of intronless transcripts. EMBO J **24:**1831-1841.
57. **Massimelli MJ, Kang JG, Majerciak V, Le SY, Liewehr DJ, Steinberg SM, Zheng ZM.** 2011. Stability of a long noncoding viral RNA depends on a 9-nt core element at the RNA 5' end to interact with viral ORF57 and cellular PABPC1. Int J Biol Sci **7:**1145-1160.

58. **Mitton-Fry RM, DeGregorio SJ, Wang J, Steitz TA, Steitz JA.** 2010. Poly(A) tail recognition by a viral RNA element through assembly of a triple helix. Science **330:**1244-1247.
59. **Massimelli MJ, Majerciak V, Kruhlak M, Zheng ZM.** 2013. Interplay between polyadenylate-binding protein 1 and Kaposi's sarcoma-associated herpesvirus ORF57 in accumulation of polyadenylated nuclear RNA, a viral long noncoding RNA. J Virol **87:**243-256.
60. **Rossetto CC, Tarrant-Elorza M, Verma S, Purushothaman P, Pari GS.** 2013. Regulation of viral and cellular gene expression by Kaposi's sarcoma-associated herpesvirus polyadenylated nuclear RNA. J Virol **87:**5540-5553.
61. **Campbell M, Kim KY, Chang PC, Huerta S, Shevchenko B, Wang DH, Izumiya C, Kung HJ, Izumiya Y.** 2014. A lytic viral long noncoding RNA modulates the function of a latent protein. J Virol **88:**1843-1848.
62. **Withers JB, Li ES, Vallery TK, Yario TA, Steitz JA.** 2018. Two herpesviral noncoding PAN RNAs are functionally homologous but do not associate with common chromatin loci. PLoS Pathog **14:**e1007389.
63. **Xiao B, Verma SC, Cai Q, Kaul R, Lu J, Saha A, Robertson ES.** 2010. Bub1 and CENP-F can contribute to Kaposi's sarcoma-associated herpesvirus genome persistence by targeting LANA to kinetochores. J Virol **84:**9718-9732.
64. **Branon TC, Bosch JA, Sanchez AD, Udeshi ND, Svinkina T, Carr SA, Feldman JL, Perrimon N, Ting AY.** 2018. Efficient proximity labeling in living cells and organisms with TurboID. Nat Biotechnol **36:**880-887.
65. **Kumar A, Salemi M, Bhullar R, Guevara-Plunkett S, Lyu Y, Wang KH, Izumiya C, Campbell M, Nakajima KI, Izumiya Y.** 2021. Proximity Biotin Labeling Reveals KSHV Interferon Regulatory Factor Networks. J Virol doi:10.1128/JVI.02049-20.
66. **Hellert J, Weidner-Glunde M, Krausze J, Richter U, Adler H, Fedorov R, Pietrek M, Ruckert J, Ritter C, Schulz TF, Luhrs T.** 2013. A structural basis for BRD2/4-mediated host chromatin interaction and oligomer assembly of Kaposi sarcoma-associated herpesvirus and murine gammaherpesvirus LANA proteins. PLoS Pathog **9:**e1003640.
67. **Verma SC, Cai Q, Kreider E, Lu J, Robertson ES.** 2013. Comprehensive analysis of LANA interacting proteins essential for viral genome tethering and persistence. PLoS One **8:**e74662.
68. **Si H, Verma SC, Lampson MA, Cai Q, Robertson ES.** 2008. Kaposi's sarcoma-associated herpesvirus-encoded LANA can interact with the nuclear mitotic apparatus protein to regulate genome maintenance and segregation. J Virol **82:**6734-6746.
69. **Lim C, Lee D, Seo T, Choi C, Choe J.** 2003. Latency-associated nuclear antigen of Kaposi's sarcoma-associated herpesvirus functionally interacts with heterochromatin protein 1. J Biol Chem **278:**7397-7405.
70. **Skene PJ, Henikoff S.** 2017. An efficient targeted nuclease strategy for high-resolution mapping of DNA binding sites. Elife **6**.
71. **Manzano M, Gunther T, Ju H, Nicholas J, Bartom ET, Grundhoff A, Gottwein E.** 2020. Kaposi's Sarcoma-Associated Herpesvirus Drives a Super-Enhancer-Mediated Survival Gene Expression Program in Primary Effusion Lymphoma. mBio **11**.
72. **Wang C, Zhang L, Ke L, Ding W, Jiang S, Li D, Narita Y, Hou I, Liang J, Li S, Xiao H, Gottwein E, Kaye KM, Teng M, Zhao B.** 2020. Primary effusion lymphoma enhancer connectome links super-enhancers to dependency factors. Nat Commun **11:**6318.
73. **Garber AC, Shu MA, Hu J, Renne R.** 2001. DNA binding and modulation of gene expression by the latency-associated nuclear antigen of Kaposi's sarcoma-associated herpesvirus. J Virol **75:**7882-7892.
74. **Purushothaman P, Thakker S, Verma SC.** 2015. Transcriptome analysis of Kaposi's sarcoma-associated herpesvirus during de novo primary infection of human B and endothelial cells. J Virol **89:**3093-3111.
75. **Arnold PR, Wells AD, Li XC.** 2019. Diversity and Emerging Roles of Enhancer RNA in Regulation of Gene Expression and Cell Fate. Front Cell Dev Biol **7:**377.
76. **Morra R, Lee BM, Shaw H, Tuma R, Mancini EJ.** 2012. Concerted action of the PHD, chromo and motor domains regulates the human chromatin remodelling ATPase CHD4. FEBS Lett **586:**2513-2521.

77. **Weiss K, Lazar HP, Kurolap A, Martinez AF, Paperna T, Cohen L, Smeland MF, Whalen S, Heide S, Keren B, Terhal P, Irving M, Takaku M, Roberts JD, Petrovich RM, Schrier Vergano SA, Kenney A, Hove H, DeChene E, Quinonez SC, Colin E, Ziegler A, Rumple M, Jain M, Monteil D, Roeder ER, Nugent K, van Haeringen A, Gambello M, Santani A, Medne L, Krock B, Skraban CM, Zackai EH, Dubbs HA, Smol T, Ghoumid J, Parker MJ, Wright M, Turnpenny P, Clayton-Smith J, Metcalfe K, Kurumizaka H, Gelb BD, Baris Feldman H, Campeau PM, Muenke M, Wade PA, Lachlan K.** 2020. The CHD4-related syndrome: a comprehensive investigation of the clinical spectrum, genotype-phenotype correlations, and molecular basis. Genet Med **22:**389-397.

78. **Hansen AS, Hsieh TS, Cattoglio C, Pustova I, Saldana-Meyer R, Reinberg D, Darzacq X, Tjian R.** 2019. Distinct Classes of Chromatin Loops Revealed by Deletion of an RNA-Binding Region in CTCF. Mol Cell **76:**395-411 e313.

79. **Saldana-Meyer R, Rodriguez-Hernaez J, Escobar T, Nishana M, Jacome-Lopez K, Nora EP, Bruneau BG, Tsirigos A, Furlan-Magaril M, Skok J, Reinberg D.** 2019. RNA Interactions Are Essential for CTCF-Mediated Genome Organization. Mol Cell **76:**412-422 e415.

80. **Nair SJ, Yang L, Meluzzi D, Oh S, Yang F, Friedman MJ, Wang S, Suter T, Alshareedah I, Gamliel A, Ma Q, Zhang J, Hu Y, Tan Y, Ohgi KA, Jayani RS, Banerjee PR, Aggarwal AK, Rosenfeld MG.** 2019. Phase separation of ligand-activated enhancers licenses cooperative chromosomal enhancer assembly. Nat Struct Mol Biol **26:**193-203.

81. **Isoda T, Moore AJ, He Z, Chandra V, Aida M, Denholtz M, Piet van Hamburg J, Fisch KM, Chang AN, Fahl SP, Wiest DL, Murre C.** 2017. Non-coding Transcription Instructs Chromatin Folding and Compartmentalization to Dictate Enhancer-Promoter Communication and T Cell Fate. Cell **171:**103-119 e118.

82. **Coe BP, Stessman HAF, Sulovari A, Geisheker MR, Bakken TE, Lake AM, Dougherty JD, Lein ES, Hormozdiari F, Bernier RA, Eichler EE.** 2019. Neurodevelopmental disease genes implicated by de novo mutation and copy number variation morbidity. Nat Genet **51:**106-116.

83. **Sifrim A, Hitz MP, Wilsdon A, Breckpot J, Turki SH, Thienpont B, McRae J, Fitzgerald TW, Singh T, Swaminathan GJ, Prigmore E, Rajan D, Abdul-Khaliq H, Banka S, Bauer UM, Bentham J, Berger F, Bhattacharya S, Bu'Lock F, Canham N, Colgiu IG, Cosgrove C, Cox H, Daehnert I, Daly A, Danesh J, Fryer A, Gewillig M, Hobson E, Hoff K, Homfray T, Study I, Kahlert AK, Ketley A, Kramer HH, Lachlan K, Lampe AK, Louw JJ, Manickara AK, Manase D, McCarthy KP, Metcalfe K, Moore C, Newbury-Ecob R, Omer SO, Ouwehand WH, Park SM, Parker MJ, Pickardt T, Pollard MO, et al.** 2016. Distinct genetic architectures for syndromic and nonsyndromic congenital heart defects identified by exome sequencing. Nat Genet **48:**1060-1065.

84. **Zhao S, Choi M, Overton JD, Bellone S, Roque DM, Cocco E, Guzzo F, English DP, Varughese J, Gasparrini S, Bortolomai I, Buza N, Hui P, Abu-Khalaf M, Ravaggi A, Bignotti E, Bandiera E, Romani C, Todeschini P, Tassi R, Zanotti L, Carrara L, Pecorelli S, Silasi DA, Ratner E, Azodi M, Schwartz PE, Rutherford TJ, Stiegler AL, Mane S, Boggon TJ, Schlessinger J, Lifton RP, Santin AD.** 2013. Landscape of somatic single-nucleotide and copy-number mutations in uterine serous carcinoma. Proc Natl Acad Sci U S A **110:**2916-2921.

85. **Le Gallo M, O'Hara AJ, Rudd ML, Urick ME, Hansen NF, O'Neil NJ, Price JC, Zhang S, England BM, Godwin AK, Sgroi DC, Program NIHISCCS, Hieter P, Mullikin JC, Merino MJ, Bell DW.** 2012. Exome sequencing of serous endometrial tumors identifies recurrent somatic mutations in chromatin-remodeling and ubiquitin ligase complex genes. Nat Genet **44:**1310-1315.

86. **Kim KD, Tanizawa H, De Leo A, Vladimirova O, Kossenkov A, Lu F, Showe LC, Noma KI, Lieberman PM.** 2020. Epigenetic specifications of host chromosome docking sites for latent Epstein-Barr virus. Nat Commun **11:**877.

87. **Carbone A, Gloghini A, Cozzi MR, Capello D, Steffan A, Monini P, De Marco L, Gaidano G.** 2000. Expression of MUM1/IRF4 selectively clusters with primary effusion lymphoma among lymphomatous effusions: implications for disease histogenesis and pathogenesis. Br J Haematol **111:**247-257.

88. **Majerciak V, Pripuzova N, McCoy JP, Gao SJ, Zheng ZM.** 2007. Targeted disruption of Kaposi's sarcoma-associated herpesvirus ORF57 in the viral genome is detrimental for the expression of ORF59, K8alpha, and K8.1 and the production of infectious virus. J Virol **81:**1062-1071.
89. **Rao SS, Huntley MH, Durand NC, Stamenova EK, Bochkov ID, Robinson JT, Sanborn AL, Machol I, Omer AD, Lander ES, Aiden EL.** 2014. A 3D map of the human genome at kilobase resolution reveals principles of chromatin looping. Cell **159:**1665-1680.
90. **Belaghzal H, Dekker J, Gibcus JH.** 2017. Hi-C 2.0: An optimized Hi-C procedure for high-resolution genome-wide mapping of chromosome conformation. Methods **123:**56-65.
91. **Schmitt AD, Hu M, Ren B.** 2016. Genome-wide mapping and analysis of chromosome architecture. Nature Reviews Molecular Cell Biology **17:**743-755.
92. **Schoenfelder S, Javierre B-M, Furlan-Magaril M, Wingett SW, Fraser P.** 2018. Promoter Capture Hi-C: High-resolution, Genome-wide Profiling of Promoter Interactions. Journal of Visualized Experiments : JoVE doi:10.3791/57320.
93. **Jung I, Schmitt A, Diao Y, Lee AJ, Liu T, Yang D, Tan C, Eom J, Chan M, Chee S, Chiang Z, Kim C, Masliah E, Barr CL, Li B, Kuan S, Kim D, Ren B.** 2019. A compendium of promoter-centered long-range chromatin interactions in the human genome. Nat Genet **51:**1442-1449.
94. **Servant N, Varoquaux N, Lajoie BR, Viara E, Chen CJ, Vert JP, Heard E, Dekker J, Barillot E.** 2015. HiC-Pro: an optimized and flexible pipeline for Hi-C data processing. Genome Biol **16:**259.
95. **Khan A, Mathelier A.** 2017. Intervene: a tool for intersection and visualization of multiple gene or genomic region sets. BMC Bioinformatics **18:**287.
96. **Wingett S, Ewels P, Furlan-Magaril M, Nagano T, Schoenfelder S, Fraser P, Andrews S.** 2015. HiCUP: pipeline for mapping and processing Hi-C data. F1000Res **4:**1310.
97. **Durand NC, Robinson JT, Shamim MS, Machol I, Mesirov JP, Lander ES, Aiden EL.** 2016. Juicebox Provides a Visualization System for Hi-C Contact Maps with Unlimited Zoom. Cell Syst **3:**99-101.
98. **Heinz S, Benner C, Spann N, Bertolino E, Lin YC, Laslo P, Cheng JX, Murre C, Singh H, Glass CK.** 2010. Simple combinations of lineage-determining transcription factors prime cis-regulatory elements required for macrophage and B cell identities. Mol Cell **38:**576-589.
99. **Langmead B, Salzberg SL.** 2012. Fast gapped-read alignment with Bowtie 2. Nat Methods **9:**357-359.
100. **Kim D, Paggi JM, Park C, Bennett C, Salzberg SL.** 2019. Graph-based genome alignment and genotyping with HISAT2 and HISAT-genotype. Nat Biotechnol **37:**907-915.
101. **Zhang Y, Liu T, Meyer CA, Eeckhoute J, Johnson DS, Bernstein BE, Nusbaum C, Myers RM, Brown M, Li W, Liu XS.** 2008. Model-based analysis of ChIP-Seq (MACS). Genome Biol **9:**R137.
102. **Freese NH, Norris DC, Loraine AE.** 2016. Integrated genome browser: visual analytics platform for genomics. Bioinformatics **32:**2089-2095.
103. **Shen L, Shao N, Liu X, Nestler E.** 2014. ngs.plot: Quick mining and visualization of next-generation sequencing data by integrating genomic databases. BMC Genomics **15:**284.
104. **Stuart T, Butler A, Hoffman P, Hafemeister C, Papalexi E, Mauck WM, 3rd, Hao Y, Stoeckius M, Smibert P, Satija R.** 2019. Comprehensive Integration of Single-Cell Data. Cell **177:**1888-1902 e1821.
105. **Izumiya Y, Izumiya C, Hsia D, Ellison TJ, Luciw PA, Kung HJ.** 2009. NF-kappaB serves as a cellular sensor of Kaposi's sarcoma-associated herpesvirus latency and negatively regulates K-Rta by antagonizing the RBP-Jkappa coactivator. J Virol **83:**4435-4446.
106. **Izumiya Y, Ellison TJ, Yeh ET, Jung JU, Luciw PA, Kung HJ.** 2005. Kaposi's sarcoma-associated herpesvirus K-bZIP represses gene transcription via SUMO modification. J Virol **79:**9912-9925.
107. **Tischer BK, Smith GA, Osterrieder N.** 2010. En passant mutagenesis: a two step markerless red recombination system. Methods Mol Biol **634:**421-430.
108. **Brulois KF, Chang H, Lee AS, Ensser A, Wong LY, Toth Z, Lee SH, Lee HR, Myoung J, Ganem D, Oh TK, Kim JF, Gao SJ, Jung JU.** 2012. Construction and manipulation of a new Kaposi's sarcoma-associated herpesvirus bacterial artificial chromosome clone. J Virol **86:**9708-9720.

109. **Fakhari FD, Dittmer DP.** 2002. Charting latency transcripts in Kaposi's sarcoma-associated herpesvirus by whole-genome real-time quantitative PCR. J Virol **76:**6213-6223.
110. **Nesvizhskii AI, Keller A, Kolker E, Aebersold R.** 2003. A statistical model for identifying proteins by tandem mass spectrometry. Anal Chem **75:**4646-4658.
111. **Zhou Y, Zhou B, Pache L, Chang M, Khodabakhshi AH, Tanaseichuk O, Benner C, Chanda SK.** 2019. Metascape provides a biologist-oriented resource for the analysis of systems-level datasets. Nat Commun **10:**1523.

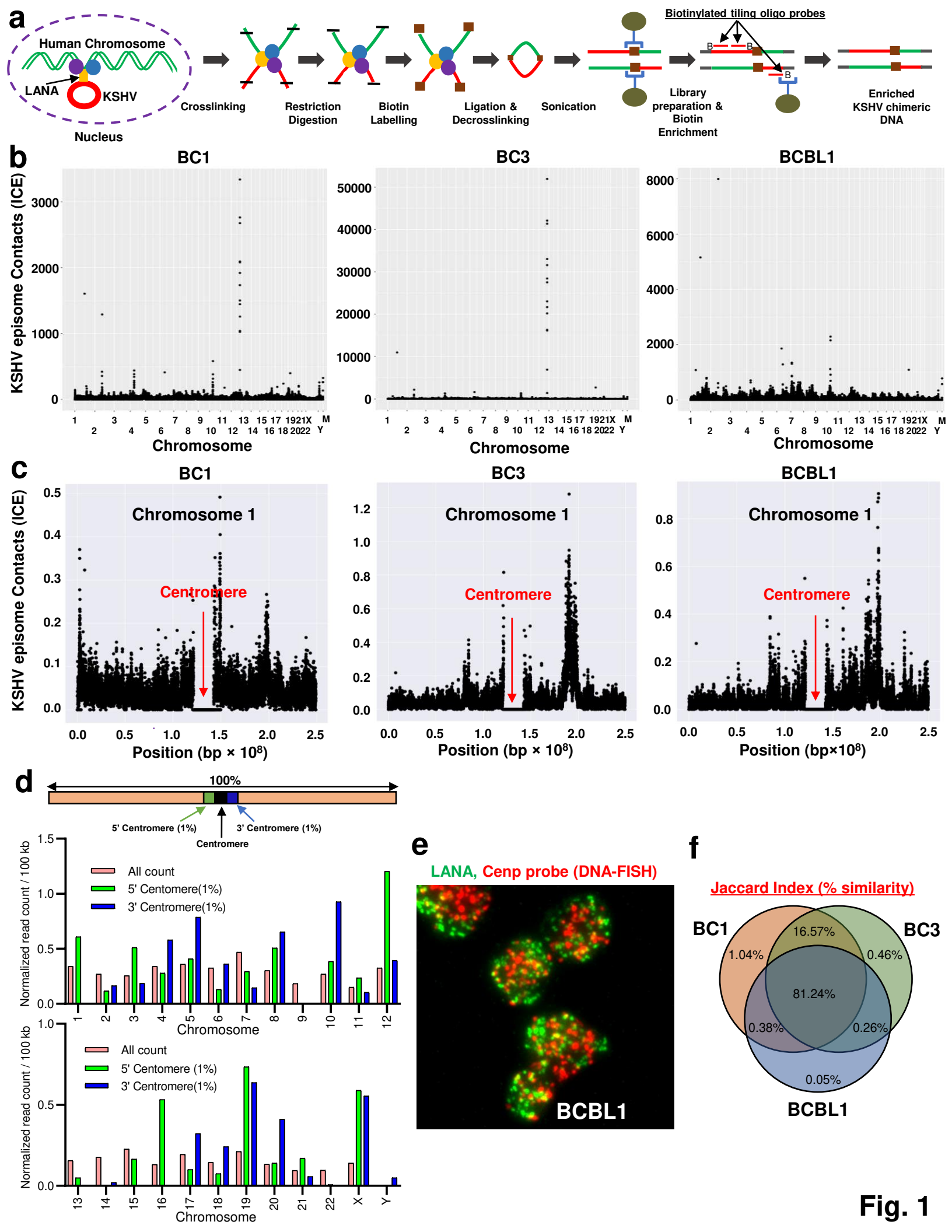
a
Human Chromosome
LANA
KSHV
Nucleus
Crosslinking
Restriction Digestion
Biotin Labelling
Ligation & Decrosslinking
Sonication
Biotinylated tiling oligo probes
Library preparation & Biotin Enrichment
Enriched KSHV chimeric DNA
b
BC1
BC3
BCBL1
KSHV episome Contacts (ICE)
Chromosome
c
BC1
BC3
BCBL1
Chromosome 1
Centromere
KSHV episome Contacts (ICE)
Position (bp × 10^8)
Position (bp×10^8)
d
100%
5' Centromere (1%)
3' Centromere (1%)
Centromere
All count
5' Centomere(1%)
3' Centromere(1%)
Normalized read count / 100 kb
Chromosome
e
LANA, Cenp probe (DNA-FISH)
BCBL1
f
Jaccard Index (% similarity)
BC1
BC3
BCBL1
16.57%
1.04%
0.46%
81.24%
0.38%
0.26%
0.05%

Fig. 1

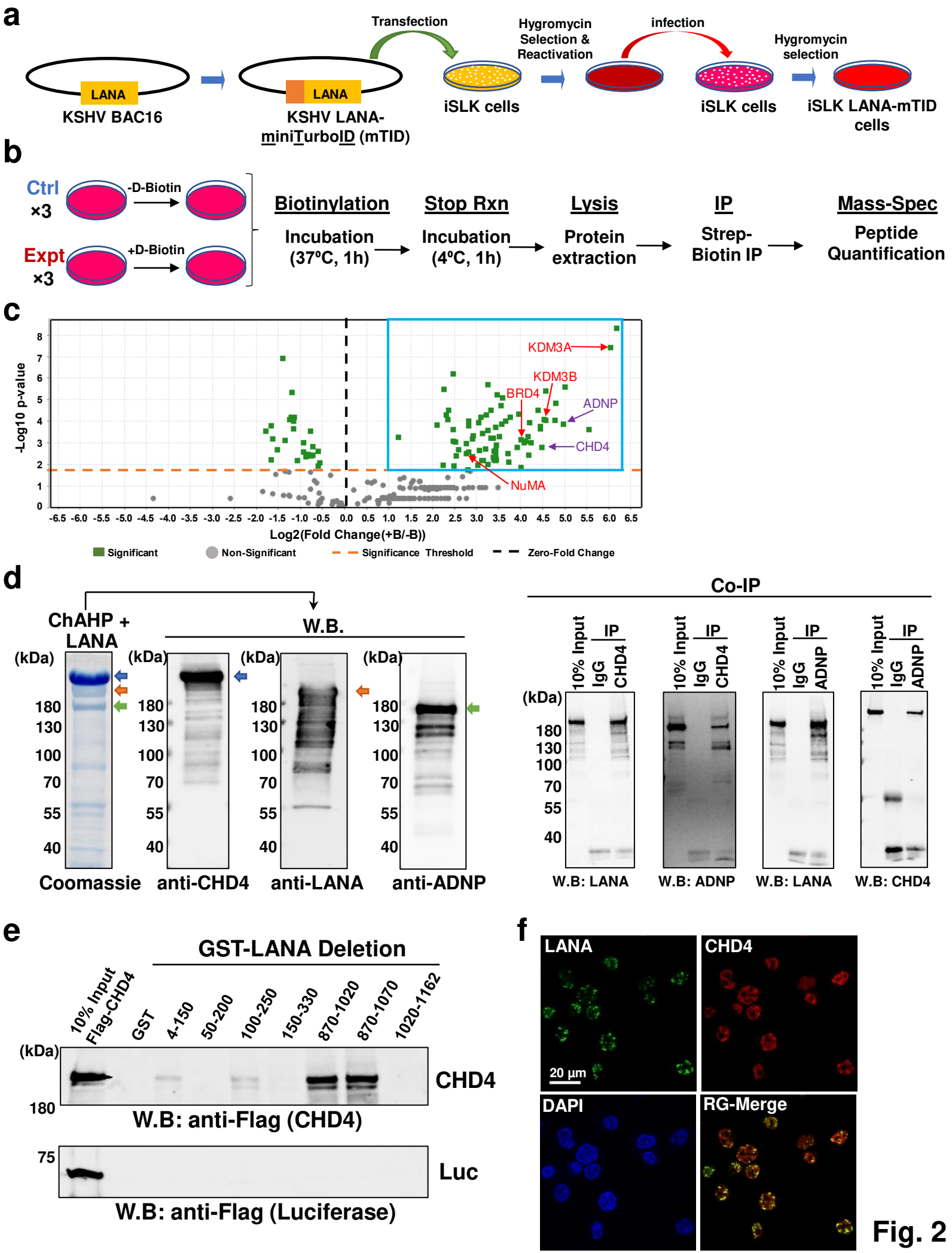
a
Transfection
Hygromycin Selection & Reactivation
infection
Hygromycin selection
LANA
KSHV BAC16
LANA
KSHV LANA-miniTurboID (mTID)
iSLK cells
iSLK cells
iSLK LANA-mTID cells
b
Ctrl ×3
-D-Biotin
Expt ×3
+D-Biotin
Biotinylation
Incubation (37ºC, 1h)
Stop Rxn
Incubation (4ºC, 1h)
Lysis
Protein extraction
IP
Strep-Biotin IP
Mass-Spec
Peptide Quantification
c
-Log10 p-value
KDM3A
KDM3B
BRD4
ADNP
CHD4
NuMA
Log2(Fold Change(+B/-B))
Significant
Non-Significant
Significance Threshold
Zero-Fold Change
d
ChAHP + LANA
W.B.
(kDa)
Coomassie
anti-CHD4
anti-LANA
anti-ADNP
Co-IP
10% Input
IgG
CHD4
ADNP
W.B: LANA
W.B: ADNP
W.B: LANA
W.B: CHD4
e
GST-LANA Deletion
10% Input Flag-CHD4
GST
4-150
50-200
100-250
150-330
870-1020
870-1070
1020-1162
CHD4
W.B: anti-Flag (CHD4)
Luc
W.B: anti-Flag (Luciferase)
f
LANA
CHD4
20 µm
DAPI
RG-Merge

Fig. 2

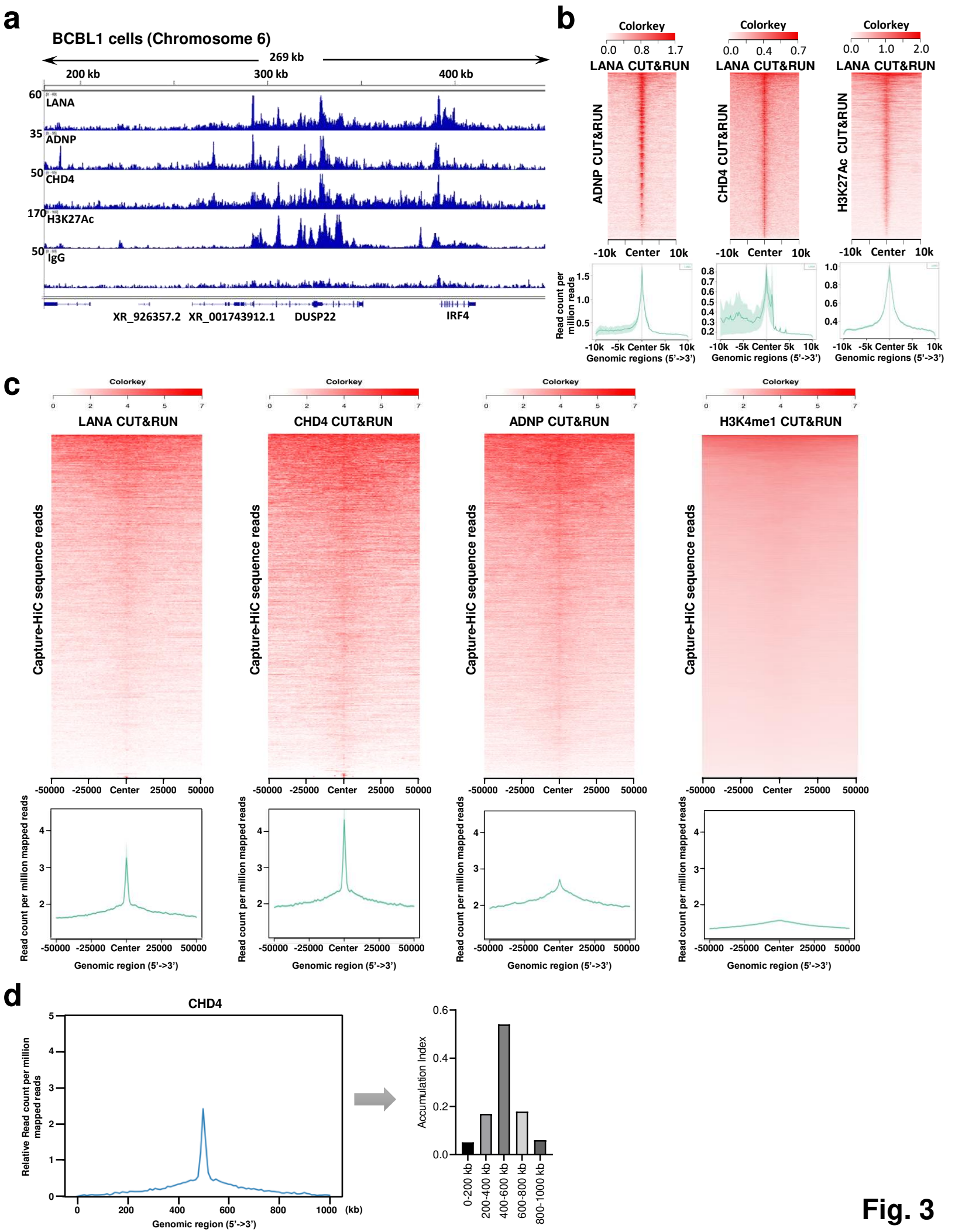
a
BCBL1 cells (Chromosome 6)
269 kb
200 kb
300 kb
400 kb
LANA
ADNP
CHD4
H3K27Ac
IgG
XR_926357.2
XR_001743912.1
DUSP22
IRF4
b
Colorkey
LANA CUT&RUN
ADNP CUT&RUN
CHD4 CUT&RUN
H3K27Ac CUT&RUN
-10k Center 10k
Read count per million reads
Genomic regions (5'->3')
c
LANA CUT&RUN
CHD4 CUT&RUN
ADNP CUT&RUN
H3K4me1 CUT&RUN
Capture-HiC sequence reads
-50000 -25000 Center 25000 50000
Read count per million mapped reads
Genomic region (5'->3')
d
CHD4
Relative Read count per million mapped reads
Genomic region (5'->3')
(kb)
Accumulation Index
0-200 kb
200-400 kb
400-600 kb
600-800 kb
800-1000 kb

Fig. 3

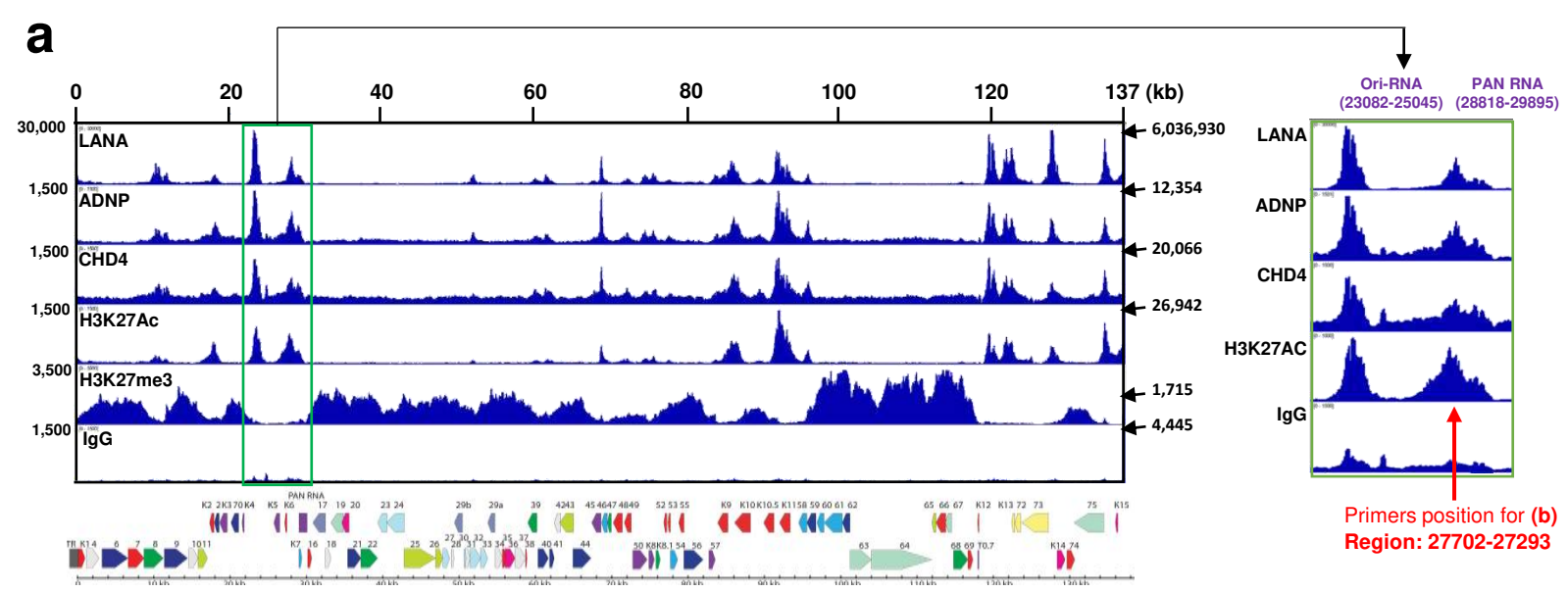
a
0
20
40
60
80
100
120
137 (kb)
30,000
LANA
6,036,930
1,500
ADNP
12,354
1,500
CHD4
20,066
1,500
H3K27Ac
26,942
3,500
H3K27me3
1,715
1,500
IgG
4,445
PAN RNA
Ori-RNA
(23082-25045)
PAN RNA
(28818-29895)
LANA
ADNP
CHD4
H3K27AC
IgG
Primers position for (b)
Region: 27702-27293

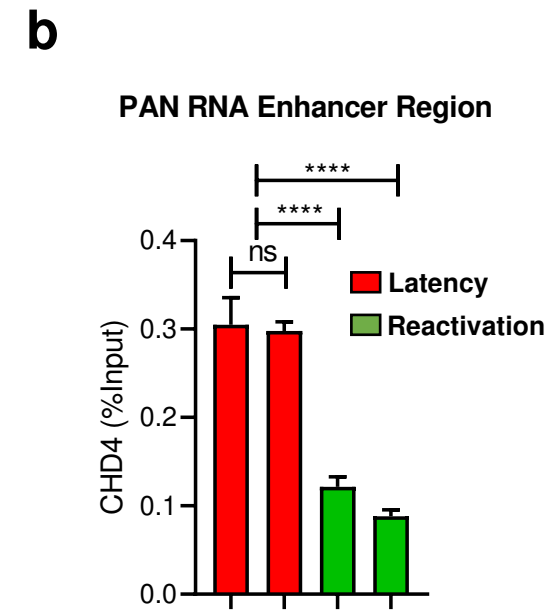
b
PAN RNA Enhancer Region
****
****
ns
Latency
Reactivation
CHD4 (%Input)
0.4
0.3
0.2
0.1
0.0

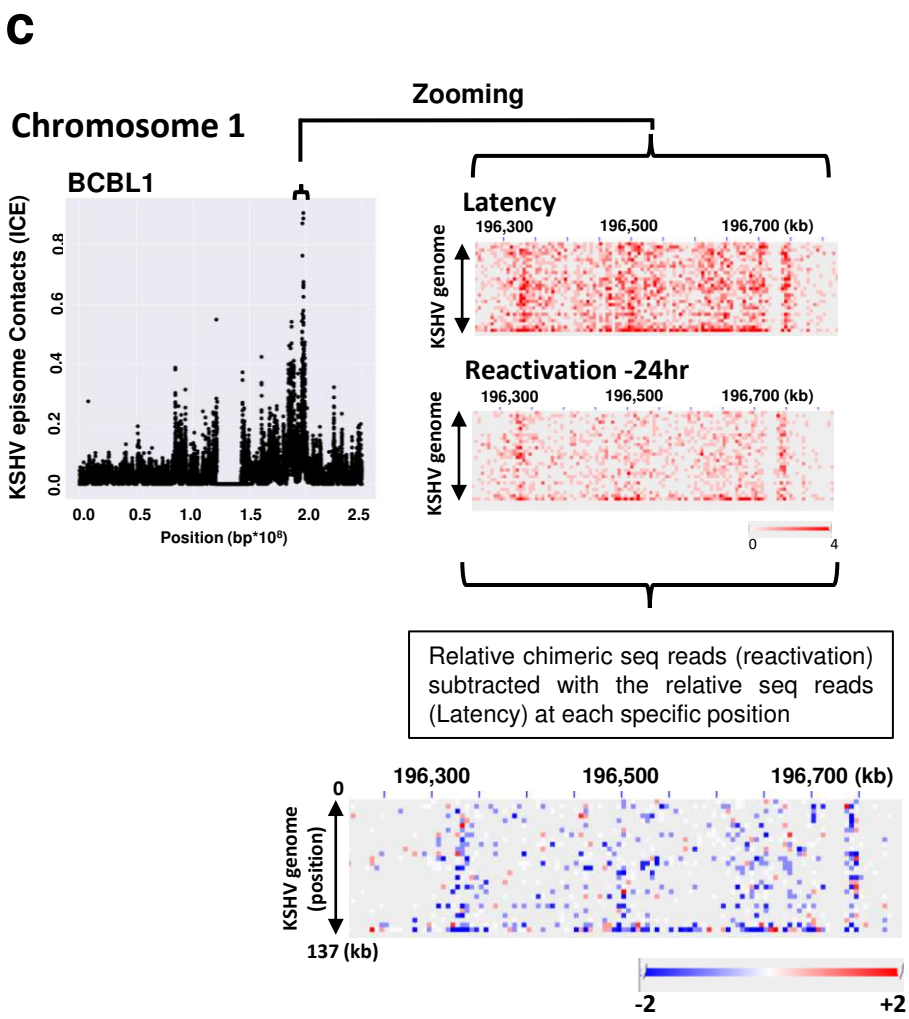
c
Chromosome 1
Zooming
BCBL1
KSHV episome Contacts (ICE)
0.0
0.2
0.4
0.6
0.8
0.0
0.5
1.0
1.5
2.0
2.5
Position (bp*10⁸)
Latency
196,300
196,500
196,700 (kb)
KSHV genome
Reactivation -24hr
196,300
196,500
196,700 (kb)
KSHV genome
0
4
Relative chimeric seq reads (reactivation) subtracted with the relative seq reads (Latency) at each specific position
196,300
196,500
196,700 (kb)
0
KSHV genome (position)
137 (kb)
-2
+2

Fig. 4

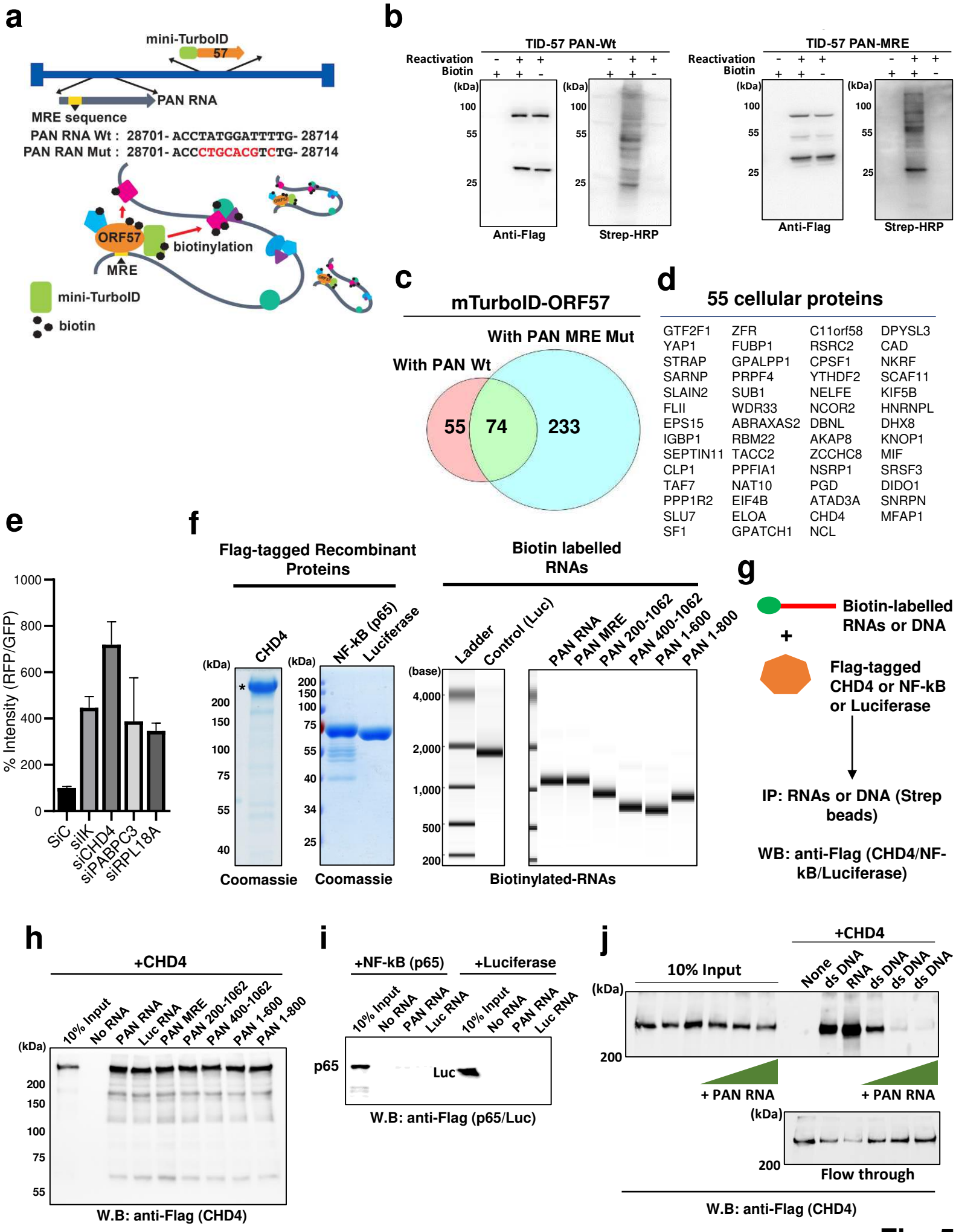
a
mini-TurboID
57
PAN RNA
MRE sequence
PAN RNA Wt : 28701- ACCTATGGATTTTG- 28714
PAN RAN Mut : 28701- ACCCTGCACGTCTG- 28714
ORF57
biotinylation
MRE
mini-TurboID
biotin
b
TID-57 PAN-Wt
TID-57 PAN-MRE
Reactivation
Biotin
(kDa)
100
55
25
Anti-Flag
Strep-HRP
c
mTurboID-ORF57
With PAN MRE Mut
With PAN Wt
55
74
233
d
55 cellular proteins
GTF2F1 ZFR C11orf58 DPYSL3
YAP1 FUBP1 RSRC2 CAD
STRAP GPALPP1 CPSF1 NKRF
SARNP PRPF4 YTHDF2 SCAF11
SLAIN2 SUB1 NELFE KIF5B
FLII WDR33 NCOR2 HNRNPL
EPS15 ABRAXAS2 DBNL DHX8
IGBP1 RBM22 AKAP8 KNOP1
SEPTIN11 TACC2 ZCCHC8 MIF
CLP1 PPFIA1 NSRP1 SRSF3
TAF7 NAT10 PGD DIDO1
PPP1R2 EIF4B ATAD3A SNRPN
SLU7 ELOA CHD4 MFAP1
SF1 GPATCH1 NCL
e
% Intensity (RFP/GFP)
1000
800
600
400
200
0
SiC
siIK
siCHD4
siPABPC3
siRPL18A
f
Flag-tagged Recombinant Proteins
Biotin labelled RNAs
CHD4
NF-kB (p65)
Luciferase
Ladder
Control (Luc)
PAN RNA
PAN MRE
PAN 200-1062
PAN 400-1062
PAN 1-600
PAN 1-800
(base)
4,000
2,000
1,000
500
200
Coomassie
Coomassie
Biotinylated-RNAs
g
Biotin-labelled RNAs or DNA
+
Flag-tagged CHD4 or NF-kB or Luciferase
IP: RNAs or DNA (Strep beads)
WB: anti-Flag (CHD4/NF-kB/Luciferase)
h
+CHD4
10% Input
No RNA
PAN RNA
Luc RNA
PAN MRE
PAN 200-1062
PAN 400-1062
PAN 1-600
PAN 1-800
W.B: anti-Flag (CHD4)
i
+NF-kB (p65)
+Luciferase
p65
Luc
W.B: anti-Flag (p65/Luc)
j
+CHD4
10% Input
None
ds DNA
RNA
ds DNA
ds DNA
ds DNA
+ PAN RNA
+ PAN RNA
Flow through
W.B: anti-Flag (CHD4)

Fig. 5

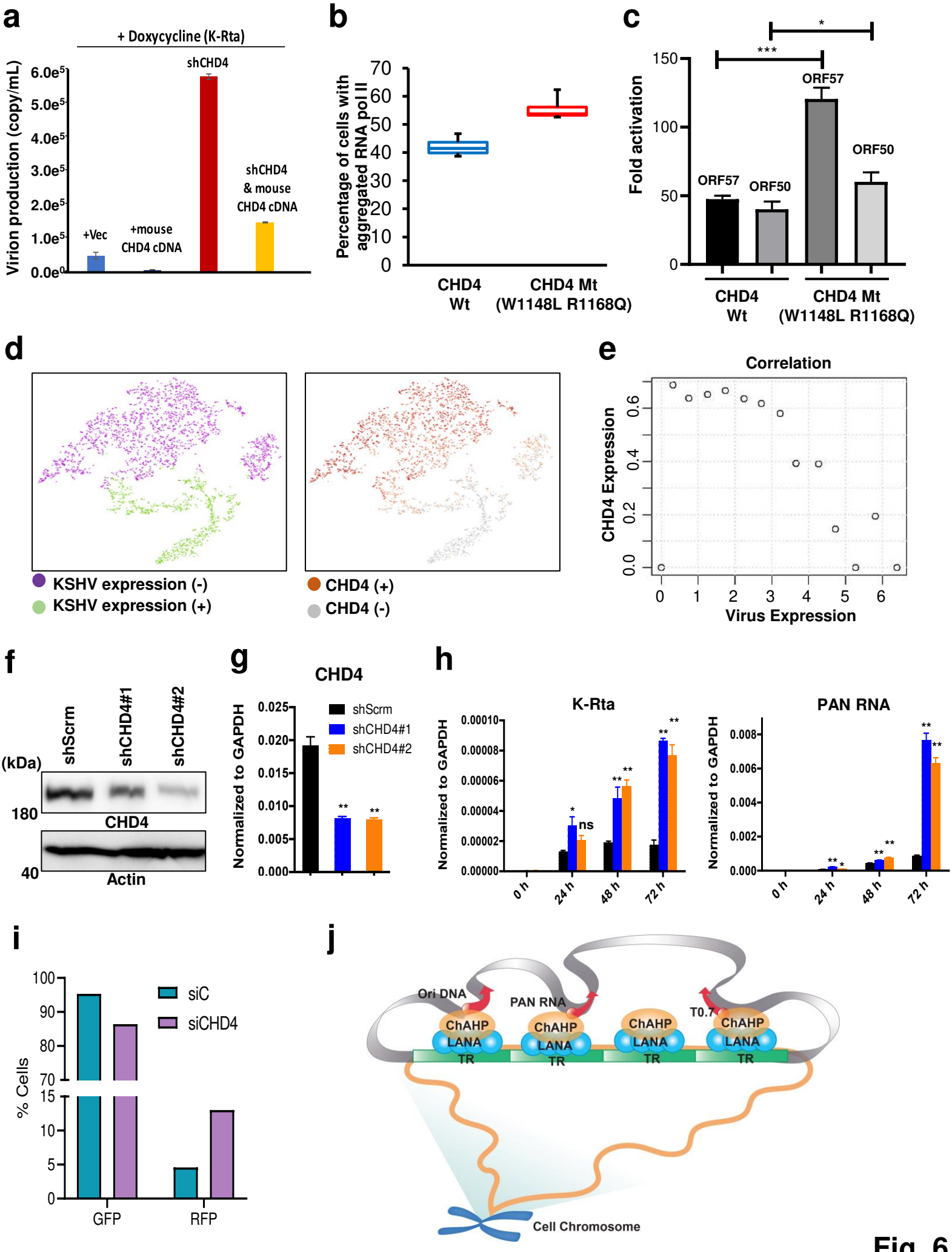
a
+ Doxycycline (K-Rta)
Virion production (copy/mL)
6.0e5
5.0e5
4.0e5
3.0e5
2.0e5
1.0e5
0.0e0
+Vec
+mouse CHD4 cDNA
shCHD4
shCHD4 & mouse CHD4 cDNA
b
Percentage of cells with aggregated RNA pol II
70
60
50
40
30
20
10
0
CHD4 Wt
CHD4 Mt (W1148L R1168Q)
c
Fold activation
150
100
50
0
***
*
ORF57
ORF50
ORF57
ORF50
CHD4 Wt
CHD4 Mt (W1148L R1168Q)
d
KSHV expression (-)
KSHV expression (+)
CHD4 (+)
CHD4 (-)
e
Correlation
CHD4 Expression
0.0
0.2
0.4
0.6
0
1
2
3
4
5
6
Virus Expression
f
(kDa)
shScrm
shCHD4#1
shCHD4#2
180
CHD4
40
Actin
g
CHD4
Normalized to GAPDH
0.025
0.020
0.015
0.010
0.005
0.000
shScrm
shCHD4#1
shCHD4#2
**
**
h
K-Rta
Normalized to GAPDH
0.00010
0.00008
0.00006
0.00004
0.00002
0.00000
*
ns
**
**
**
**
0 h
24 h
48 h
72 h
PAN RNA
Normalized to GAPDH
0.008
0.006
0.004
0.002
0.000
**
*
**
**
**
**
0 h
24 h
48 h
72 h
i
% Cells
100
90
80
70
15
10
5
0
siC
siCHD4
GFP
RFP
j
Ori DNA
PAN RNA
T0.7
ChAHP
LANA
TR
ChAHP
LANA
TR
ChAHP
LANA
TR
ChAHP
LANA
TR
Cell Chromosome

Fig. 6

Figures

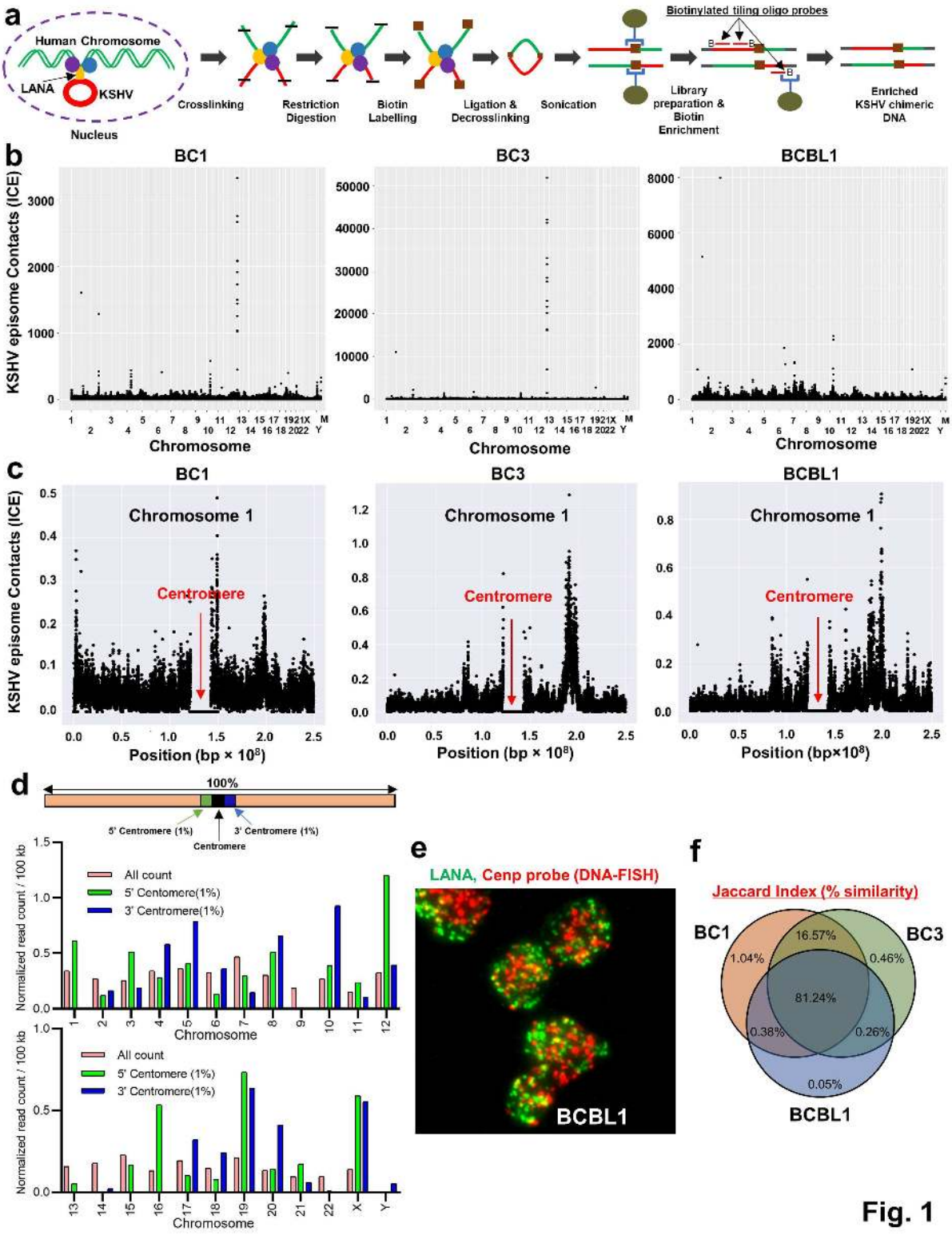

Fig. 1

Figure 1

Fig. 1 KSHV episome-tethering sites in KSHV positive cell lines. (a) Schematic workflow for Capture-HiC (CHi-C). (b) KSHV episome-docking sites on host cell chromosomes. CHi-C chimeric DNA ligation products composed of sequences derived from the KSHV and human genomes were mapped in three

naturally-infected PEL cells. For BCBL-1 cells, three biological replicates were performed with nearly identical results (similarity 0.95). M, mitochondrial chromosome. ICE-corrected profiles depicting sums of filtered read counts binned at 10 kb resolution are shown. (c) Selected chromosome 1 in zoomed view. Chromosome 1 dot plots were depicted, which displays enrichment of sequence reads near the centromere. Red arrows indicate the position of the centromere. Extended panels for all other individual chromosome for three cell lines are presented in Supplementary Fig. 1a-c. (d) KSHV episomes preferentially localize near the centromere. KSHV episome contacts were calculated in BCBL-1 cells for sequence reads in 1% (length of the respective chromosome) of the 5’-and 3'- centromere and compared with the average of the total chromosome read count. (e) LANA protein locates near the centromere. DNA-FISH was used to visualize the location of the centromere (red) and KSHV episomes were indirectly visualized by staining LANA dots (Green) in BCBL-1 cells. The centromere and LANA were probed using a Cenp probe and anti-LANA antibody respectively with IFA. The two signals were frequently co-localized, and 3D view and their image analyses are presented in Supplementary Fig. 2. (f) Jaccard statistics and Venn diagram. Venn diagram shows percent similarity of KSHV episome-tethering positions among BC-1, BC-3 and BCBL-1 cells.

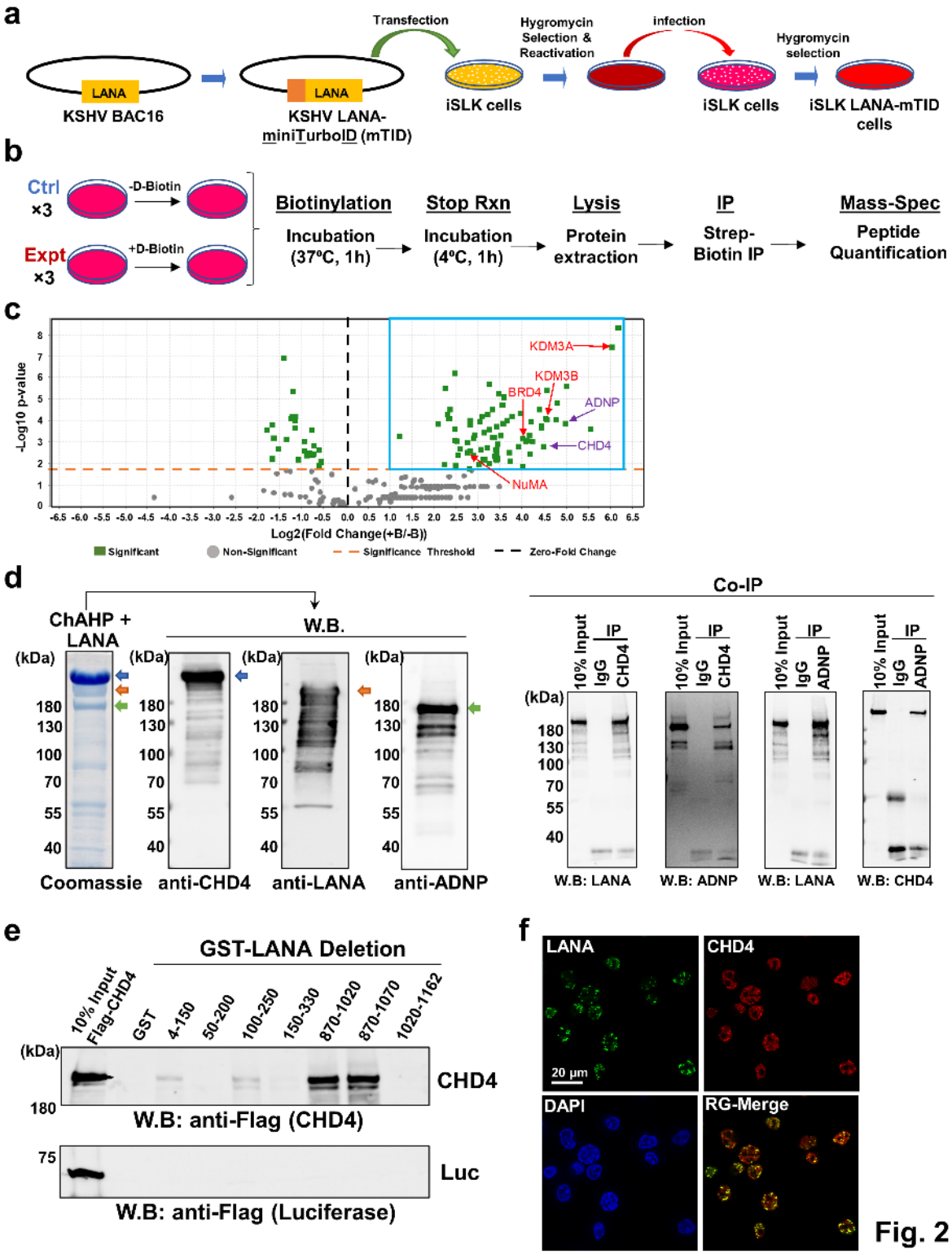

Fig. 2

Figure 2

LANA interacts with the ChAHP complex. (a) A schematic diagram of preparation of recombinant KSHV infected iSLK cells. A mini-TurboID (mTID) was fused to the N-terminus of the LANA open reading frame to generate KSHV LANA-mTID. KSHV LANA-mTID was transfected into iSLK cells followed by production of viral particles by stimulating cells with doxycycline (1 µg/ml) and sodium butyrate (3 mM) for 5 days. Virus was used to infect iSLK cells and cells were selected with hygromycin (1 mg/ml) to obtain an iSLK-

LANA mTID stable cell line. (b) Experimental design for preparing samples for protein ID. iSLK-LANA mTID cells were left un-incubated (-) or incubated (+) with D-Biotin (500 μM) for 1 hr. Unincubated (-) cells were used as control samples. Each protein ID was performed in three biological replicates. (c) Volcano plot depicting proteins in close proximity to LANA. The volcano plot represents proteins identified in close proximity to LANA. Proteins with an abundance Log2 FC of greater than or equal to 1 and p-value less than 0.05 were selected and are shown by blue box. T-test was used for calculating the p-value. Purple color; ChAHP components. Red color; previously identified proteins as LANA interacting proteins. (d) LANA interacts with CHD4 and ADNP in vitro. LANA, CHD4 and ADNP complex, which consists of Flag-LANA (gold arrow), Flag-CHD4 (blue arrow), and His-ADNP (green arrow) was prepared by co-infected three recombinant baculoviruses, and the protein complex was isolated in the presence of 500 mM NaCl and 10% glycerol with affinity purification. The authenticity of respective protein band was confirmed by immunoblotting with specific antibodies. Coomassie staining is shown. An equimolar amount (100 nM) of the three proteins were incubated in binding buffer and immunoprecipitated with the specific antibodies of one another. Ten percent of the reaction before immunoprecipitation was shown as controls. W.B: Western Blotting, Co-IP: Co-immunoprecipitation. (e) CHD4 interaction site on LANA. Purified GST-tagged LANA deletions, Flag-tagged luciferase and 41 Flag-tagged CHD4 were prepared from recombinant baculovirus infected Sf9 cells. An equal amount (1 μg) of each LANA deletion protein was incubated with full length Flag-tagged luciferase (1 μg) or Flag-tagged CHD4 (1 μg) in binding buffer and interaction was probed with anti-Flag antibody. LANA deletion proteins used for this GST-pull down assay are presented in 910 Supplementary Fig. 4. (f) LANA co-localizes with CHD4 in BCBL-1. CHD4 and LANA were 911 probed with anti-CHD4 rabbit monoclonal antibody and anti-LANA rat monoclonal antibody, 912 respectively. Images were taken with Keyence fluorescence microscopy. Scale bar (20 μm) is 913 shown

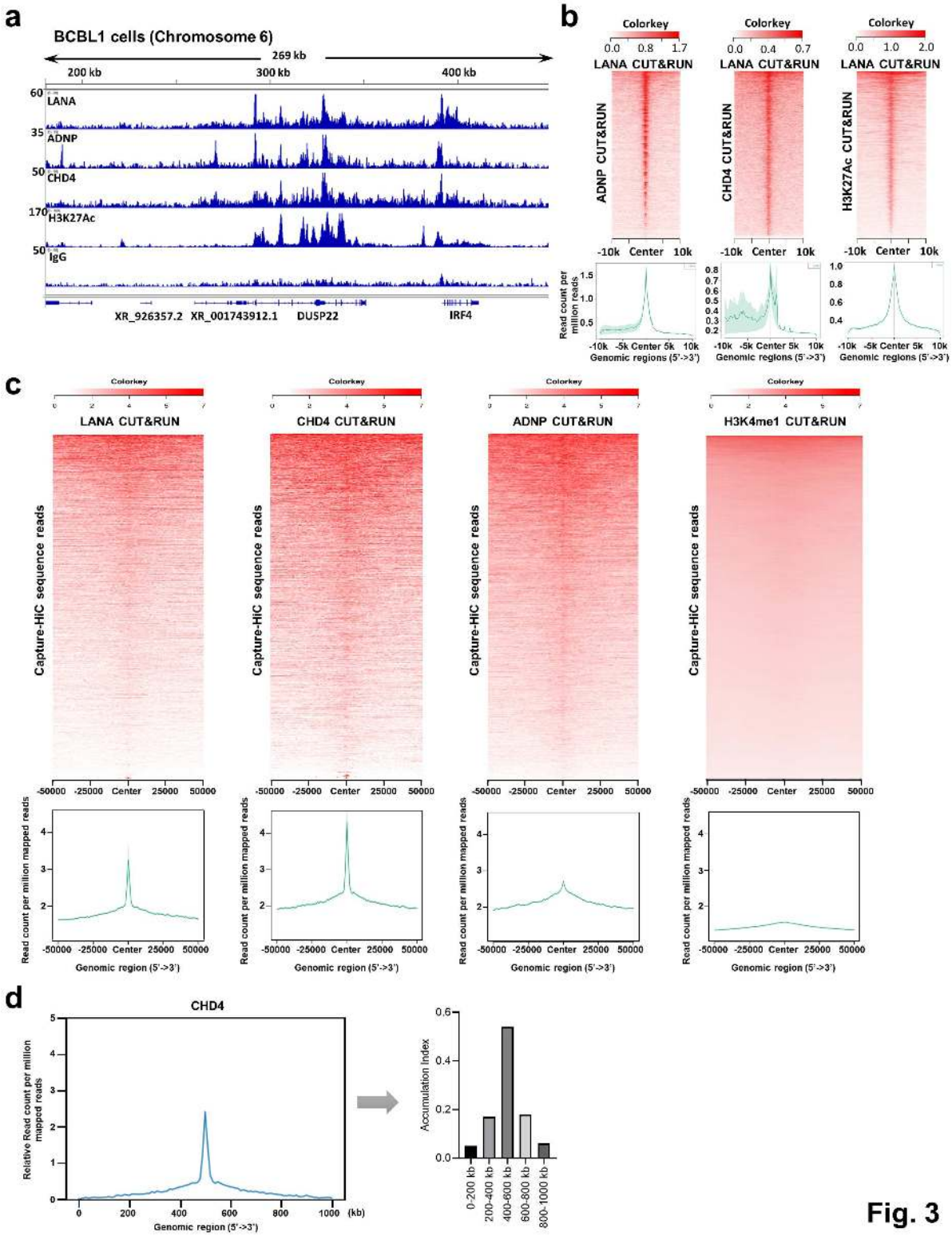

Fig. 3

Figure 3

Association of ChAHP complex binding with KSHV episome-tethering sites. (a) CUT&RUN analysis for LANA, ADNP, CHD4 and H3K27Ac. The indicated antibodies were used for CUT&RUN in BCBL-1 cells. CUT&RUN peaks were visualized with Integrative Genomics Viewer (IGV) and a snapshot of one of the major binding sites (IRF4 super enhancer region) is shown. The number on the left-hand side denotes the height of the peak (e.g., read depth) and the number along the top denotes the positions on chromosome

6. (b) Heatmaps for co-occupancies of LANA with ADNP, CHD4 and H3K27Ac on chromosomes. Heatmap (middle) and average profile (bottom) showing correlation of LANA enrichment (by color intensity and region) with ADNP, CHD4, and H3K27Ac occupancies. Average profile plot summarizing the heatmap (bottom). The lighter green shade represents the standard error (SEM) on the average profile plot. Color keys are shown on the each heatmap (top). (c) Heatmaps for correlation of CHi-C with CUT&RUN signals. The association between CHi-C chimeric reads and LANA, CHD4, ADNP and H3K4me1 CUT&RUN peaks were depicted as heatmap and average profile plot. (d) Accumulation index around CHD4 binding sites. The accumulation 42 of CHD4 is displayed as a proportion of area under the curve of the relative average profile. Association between distance from CHD4 summit peak and relative chimeric sequence counts is shown as a bar chart.

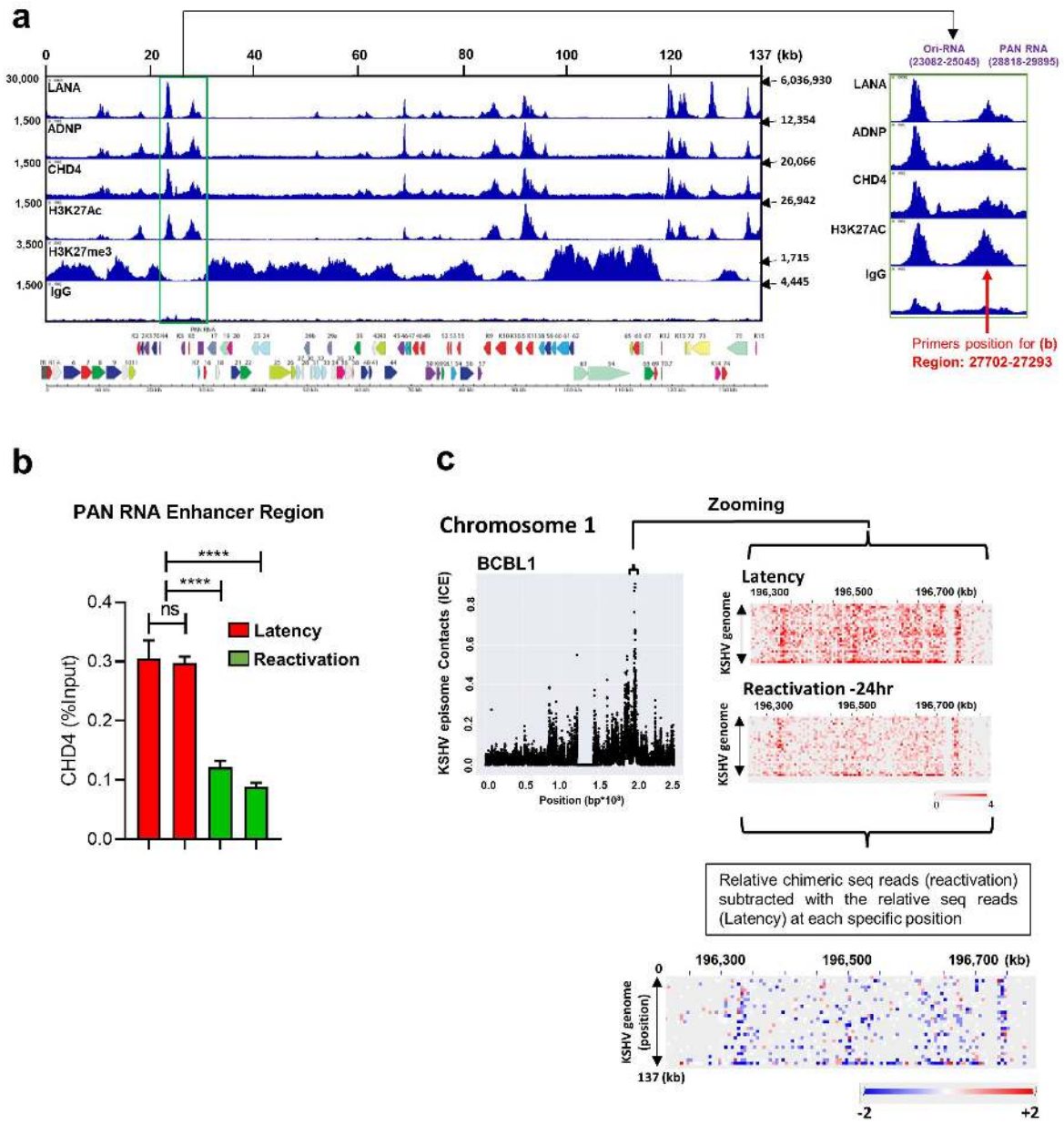

Fig. 4

Figure 4

LANA, CHD4 and ADNP colocalize on the KSHV genome. (a) CUT&RUN analysis. The indicated antibodies were used for CUT&RUN in BCBL-1 cells and sequence reads were mapped to the KSHV genome. An IGV snapshot and KSHV genome map are shown. The number on the left-hand side denotes the height of the peak (e.g., read depth), the number along the top denotes the position on KSHV genome in kilobase (kb) and the number on the right-hand side indicated by arrow denote the height of the peak on terminal

repeat region (TR). Selected region is zoomed in to show Ori-RNA and PAN RNA region. Primer used in Fig. 4b is also shown with red arrows and number show the exact location of the amplified region by the primers. (b) Regulation of CHD4 on the KSHV episome during reactivation. TREx-BCBL-1 cells were reactivated with doxycycline (1 μg/ml) and sodium butyrate (3 mM) for 24 hrs. CUT&RUN was performed on un-reactivated (latency) and reactivated cells for CHD4. CHD4 binding on the PAN RNA promoter region (red arrow in Fig. 4a, right panel) was calculated relative to the input sample (n=3, two biological replicates are shown). (c) Detachment of KSHV episomes by reactivation. BCBL-1 cells were reactivated with doxycycline (1 μg/ml) and TPA (20 nM) for 24 hrs. Chimeric sequence reads for un-reactivated (latency) and reactivated cells were mapped to the host chromosomes and visualized by Juicebox. Relative KSHV episome tethering during reactivation for the selected region on chromosome 1 was calculated by subtracting relative chimeric sequence reads in latency from relative chimeric sequence reads during reactivation. Blue and red dots indicate decreased and increased chimeric sequence reads respectively.

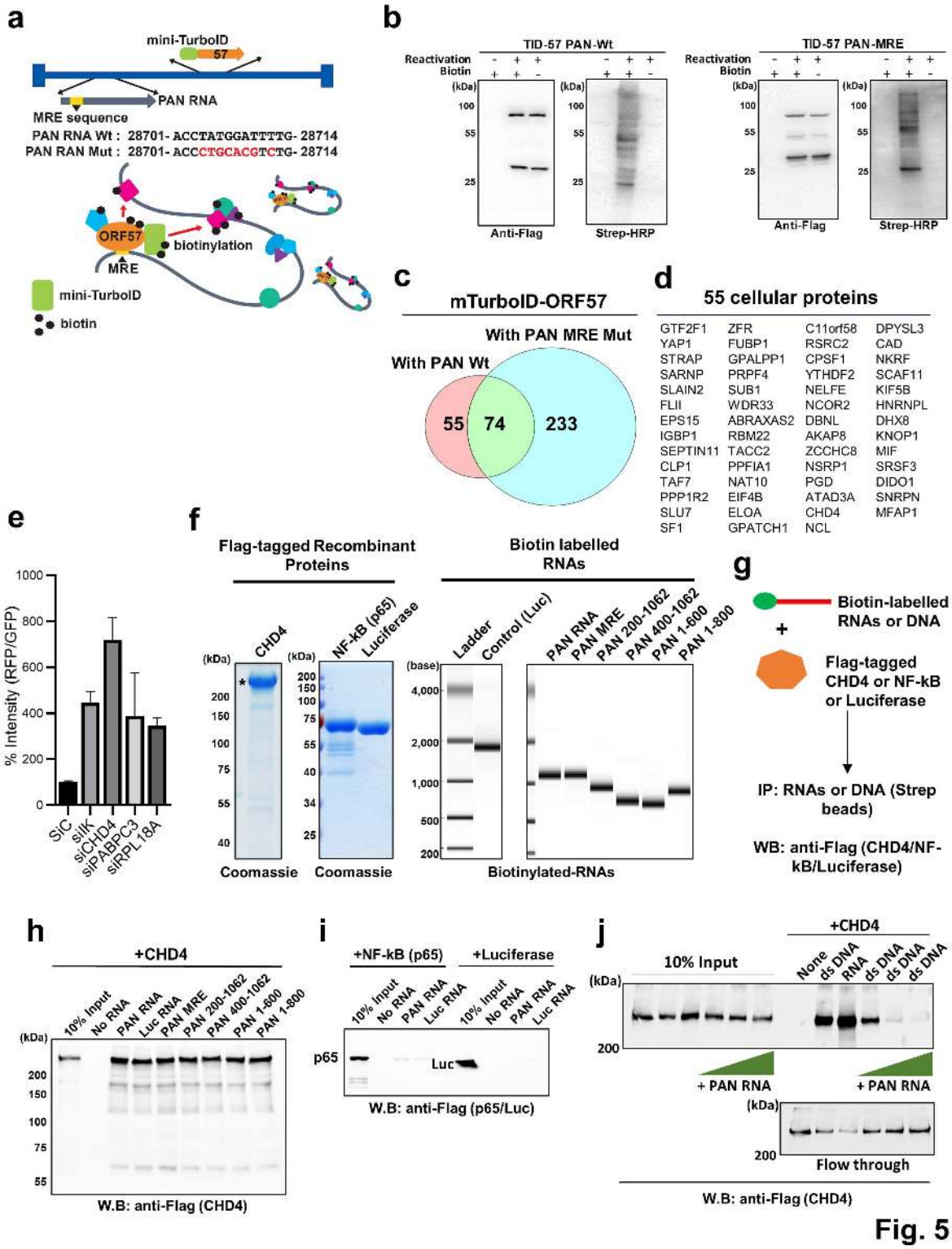

Figure 5

CHD4 is both an RNA and DNA binding protein. (a) A schematic diagram ofrecombinant KSHVs. Mini-TurboID is fused to the N-terminus of ORF57 open reading frame and the ORF57 binding site (MRE) of PAN RNA was mutated as shown. (b) Immunoblotting. Recombinant KSHV infected iSLK cells (TID-57 PAN-Wt and -MRE) were either untreated or induced for reactivation with doxycycline (1 µg/ml) and TPA (20 nM) for 24 hrs. Blots were probed with either anti-Flag antibody (for mini-TurboID-ORF57) or

Streptavidin-HRP (for biotinylated proteins). (c) Venn diagram. The Venn diagram indicates the number of identified proteins with a P value less than 0.05. Each protein ID was performed in three biological replicates. (d) PAN RNA-mediated interacting proteins with ORF57. The proteins found enriched in PAN RNA962 WT samples are shown. The entire list of proteins and peptide counts are presented in Supplementary Table 2. (e) siRNA screening with KSHV reactivation as readout. Recombinant KSHV reactivation, which encodes RFP under control of the PAN RNA promoter, was used to screen the effects of KSHV reactivation. RFP signal intensity was measured with Image J, and the GFP signal was used as internal controls. Three randomly selected fields in the middle of each well were quantified and the average intensity was plotted. (f) Recombinant proteins and synthesized PAN RNAs. Recombinant Flag-tagged proteins were expressed with baculovirus and purified with Flag-agarose beads. Coomassie staining of Flag-CHD4, Flag-NF970 kB (p65), and Flag-luciferase used for pull-down studies are shown. (g) Schematic for in vitro interaction assay performed in Fig. 5 (h-j). (h) CHD4 binds RNAs in a sequence972 independent manner. RNA pull-down was performed with the indicated biotinylated PAN RNA deletions, mutation (MRE), and irrelevant RNA (luciferase mRNA), and interaction was probed by immunoblotting with anti-Flag antibody. Beads alone (No RNA) was used for background 44 control. (i) RNA pull down was performed with indicated biotinylated RNAs, and p65 and Luciferase (Luc) were visualized by using anti-Flag antibody. (j) PAN RNA competes with CHD4 DNA binding. Pull-down analyses with biotinylated ssRNA or dsDNA was performed. CHD4 (100 nM) was incubated with biotinylated RNA (100 nM) or biotinylated dsDNA (100 nM) in 40 µL binding buffer. Increasing amounts of non-biotinylated PAN RNA at 1:1, 1:10, and 1:20 (dsDNA vs. ssRNA) were also incubated, and precipitated CHD4 protein in the pull-down was probed with anti-Flag antibody. Flow-through and 10% of the input reaction before pull-down were used as control.

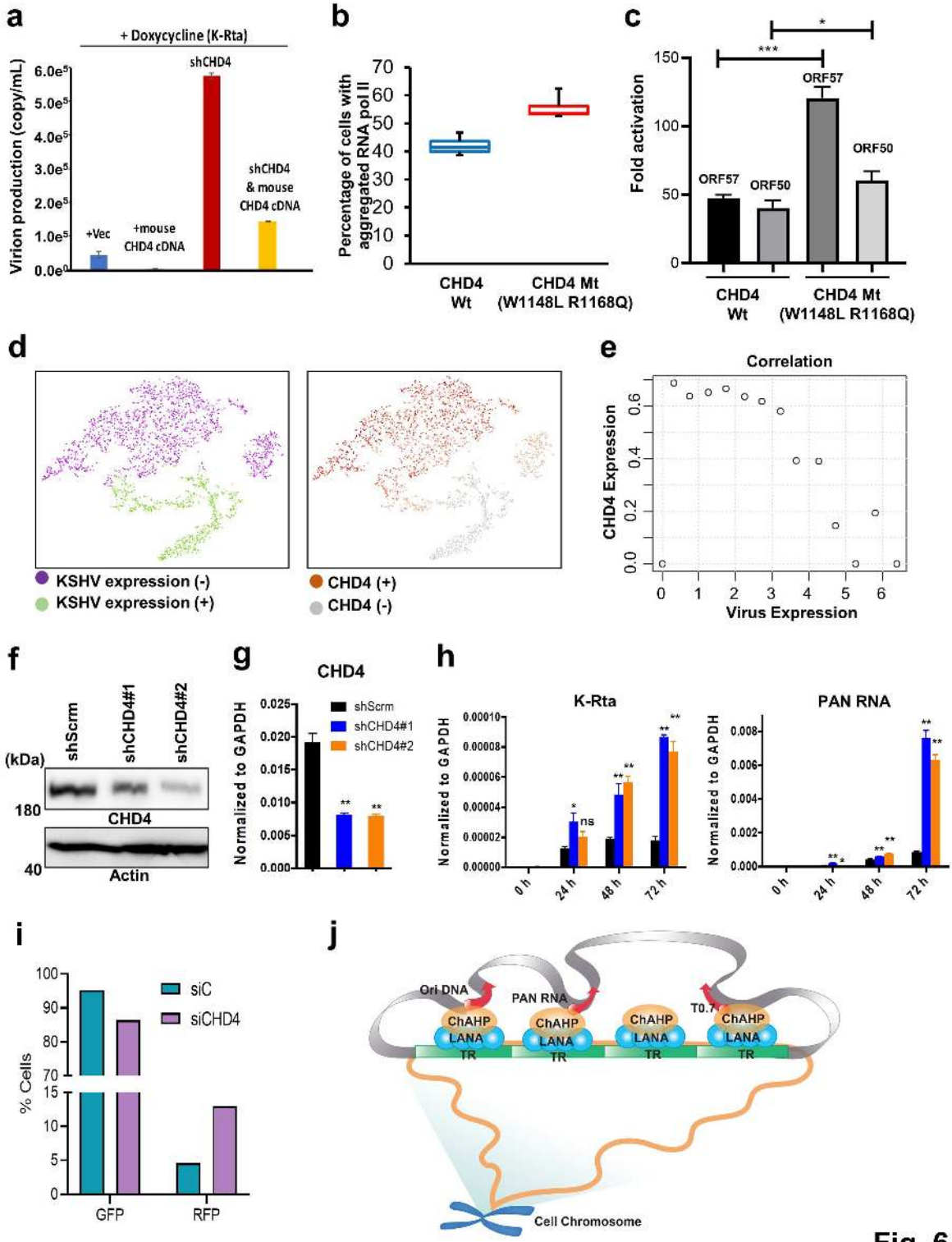

Fig. 6

Figure 6

CHD4 is important for latency maintenance and establishment. (a) CHD4 overexpression, knockdown and complementation. The iSLK.219 cell line was transfected with empty vector (Vec) or mouse CHD4 cDNA or human CHD4 shRNA, or CHD4 shRNA and mouse CHD4 cDNA for 48 hrs followed by KSHV reactivation with doxycycline (1 μg/ml) for 5 days. Encapsidated KSHV genomes in the culture supernatants were measured by qPCR to assess effects of CHD4 overexpression or knockdown on KSHV

reactivation. (b) CHD4 ATPase activity is important for prevention of nuclear aggregate formation. iSLK cells latently infected with BAC16-Wt was transfected with Flag-tagged mouse wild type CHD4, or an ATPase domain mutant was transfected and stained with anti-Flag. Transcriptional factory formation was assessed by staining RNAII. The percentage of aggregate formation in Flag-positive cells was measured and plotted. Three biological replicates were performed, and 50 cells were counted in each of the three biological replicates. (c) CHD4 ATPase activity is important for inhibiting viral gene expression during reactivation. iSLK.219 cells were transduced with an equal amount of CHD4 wild type (wt) and CHD4 mutant (mt) lentivirus for 2 days. Cells were 45 reactivated with doxycycline (1 μg/ml) for 2 days and ORF50 and ORF57 gene expression was quantified by RT-qPCR. Untreated cells were used for calculating the relative expression of ORF50 and ORF57. GAPDH was used as a negative control. *p<0.05, ***p<0.001 (comparing with CHD4 Wt). (d-e) Single cell sequencing. iSLK.219 cells were reactivated by induction of K-Rta expression from doxycycline inducible promoter for 24 hrs. Single-cell sequencing was performed with the 10x Genomics platform. A cell suspension was prepared followed by cell partitioning and 3' cDNA synthesis on the Chromium Controller and dual-index library preparation with 10x Genomics kitted reagents. (d) tSNE. tSNE was applied to separate cell clusters and KSHV gene (d, left panel) and CHD4 (d, right panel) expressing cells were marked. (e) Negative correlation between CHD4 and viral gene expression. Cells were divided into groups based on the amount of KSHV transcripts. A table and distribution of cell numbers and amount of KSHV transcripts are shown in Supplementary Fig. 6a-b. Intervals used to separate cell groups are also listed in Supplementary Fig. 6b. A correlation was established based on CHD4 expression in different groups of KSHV transcripts. (f-h) CHD4 knockdown and KSHV lytic gene expression during de novo infection. 293T cells were transduced with scramble shRNA (shScrm) or shCHD4 and stably selected with antibiotic. Immunoblot (f) and RT-qPCR (g) analysis of CHD4 in the 293T stable cell lines are shown. 293T stable cells were infected with rKSHV.219 for 24 hrs and total RNA was harvested at the indicated time points. (h) K-Rta and PAN RNA, was measured by RT-qPCR and normalized to GAPDH. *p<0.05, **p<0.01 (comparing with shScrm). (i) Flow cytometry. 293T cells were transfected with control siRNA (siC) or CHD4 siRNA (siCHD4) for 48 hrs followed by infection with rKSHV.219 virus for 96 hrs. Flow cytometry analysis was performed to calculate the number of GFP- and RFP-positive cells in siC and siCHD4 knockdown cells. (j) KSHV latency model with ChAHP. KSHV episomes 46 tether at epigenetically active regions with the ChAHP complex, and TR-loaded LANA/ChAHP prevents robust viral lncRNA expression. The action of robust lncRNA expression in lytic KSHV infection functions as an enhancer for viral ORFs that are physically neighboring with lncRNA genomic regions. Stimulation of K-Rta, in part by decreased CHD4 expression, triggers robust PAN RNA expression in the presence of ORF57, which competes with CHD4 DNA binding to enhance KSHV reactivation and detach KSHV episomes from CHD4-enriched host chromosome regions.

Supplementary Files

This is a list of supplementary files associated with this preprint. Click to download.

- SupplementaryFigures.pdf

- SupplementaryTable1.xls
- SupplementaryTable2.xls
- SupplementaryTable3.xls